1

FUNDAMENTAL CONSIDERATIONS

MILAN PAUNOVIC,[1] MORDECHAY SCHLESINGER,[2] AND DEXTER D. SNYDER[3]

COPYRIGHTED MATERIAL

1.1 INTRODUCTION

Already in the preparation of the fourth edition of *Modern Electroplating*, we realized that the first chapter in the third edition (1974) needed to be enlarged considerably in order to cover all the significant progress made since 1974. As the prospect of adding material to the chapter on fundamentals began to suggest an inbalance in the new edition, we chose to publish a separate volume titled *Fundamentals of Electrochemical Deposition (Fundamentals* in further text) that would treat the basic aspects of electrochemical deposition [1]. For this reason we provided in the fourth and now in the present fifth edition only a brief review of these fundamentals. The number of references in this chapter is also limited, and the reader is urged to consult the more extensive list of references given in both editions of *Fundamentals*.

This chapter is divided into three parts. Part A treats electrochemical aspects, part B treats physical aspects, and part C treats material science. For this presentation of the fundamentals our objective is to provide the basis for understanding only the electrochemical deposition processes treated in this volume. Information on a higher level is presented in the *Funamentals* volume.

PART A ELECTROCHEMICAL ASPECTS

In Part A we discuss (1) electrode potential, (2) kinetics and mechanism of electrodeposition, (3) growth mechanism, and (4) electroless and displacement depositions. All four topics are presented in a concise manner that emphasizes the most important points. Most concepts are clarified by solutions of numerical examples. These examples are useful for this chapter and for the chapters that follow.

1.2 ELECTRODE POTENTIAL

When a metal M is immersed in an aqueous solution containing ions of that metal, M^{z+} (e.g., salt MA), there will be an exchange of metal ions M^{z+} between two phases, the metal and the solution. Some M^{z+} ions from the crystal lattice enter the solution, and some ions from the solution enter the crystal lattice. Initially one of these reactions may occur

[1] Milan Paunovic, Part A.
[2] Mordechay Schlesinger, Part B.
[3] Dexter D. Synder, Part C.

Modern Electroplating, Fifth Edition Edited by Mordechay Schlesinger and Milan Paunovic
Copyright © 2010 John Wiley & Sons, Inc.

faster than the other. Let us assume that conditions are such that more M^{z+} ions leave than enter the crystal lattice. In this case there is an excess of electrons on the metal and the metal acquires negative charge, q_M^- (charge on the metal per unit area). In response to the charging of the metal side of the interphase, there is also a rearrangement of charges on the solution side of the interphase. The negative charge on the metal attracts positively charged M^{z+} ions from the solution and repels negatively charged A^{z-} ions. The result of this is an excess of positive M^{z+} ions in the solution in the vicinity of the metal interphase. Thus, in this case, the solution side of the interphase acquires opposite and equal charge, q_s^+ (the charge per unit area on the solution side of the interphase). This positive charge at the solution side of the interphase slows down the rate of M^{z+} ions leaving the crystal lattice (due to repulsion) and accelerates the rate of ions entering the crystal lattice. After a certain period of time a dynamic equilibrium between the metal M and its ions in the solution will result:

$$M^{z+} + ze \leftrightarrows M \tag{1.1a}$$

where z is the number of electrons involved in the reaction. Reaction from left to right consumes electrons and is called reduction. Reaction from right to left liberates electrons and is called oxidation. At the dynamic equilibrium the same number of M^{z+} ions enter, $\vec{n}$, and the same number of M^{z+} ions leave the crystal lattice, $\vec{n}$, (see Fig. 1.1):

$$\vec{n} = \overleftarrow{n} \tag{1.1b}$$

The interphase region is neutral at equilibrium:

$$q_M = -q_S \tag{1.1c}$$

The result of the charging of the interphase is the potential difference, $\Delta\phi$ (M, S), between the potentials of the metal,

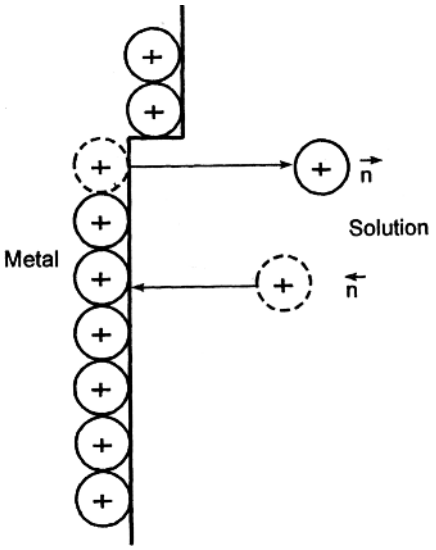

FIGURE 1.1 Formation of metal–solution interphase; equlibrium state: $\vec{n} = \vec{n}$.

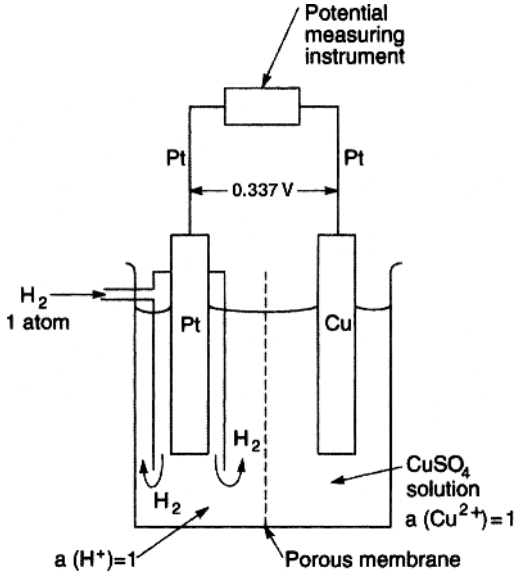

FIGURE 1.2 Relative standard electrode potential E^0 of a Cu/Cu^{2+} electrode.

ϕ_M, and the solution, ϕ_S:

$$\Delta\phi(M, S) = \phi_M - \phi_S \tag{1.2}$$

In order to measure the potential difference of an interphase, one must connect it to another one and thus form an electrochemical cell. The potential difference across this electrochemical cell can be measured.

For example, consider the cell shown in Figure 2.2. This cell may be schematically represented in the following way:

$$Pt, H_2(p = 1)|H^+(a = 1)||Cu^{2+}(a = 1)|Cu|Pt$$

where the left-hand electrode is the normal hydrogen reference electrode; a stands for activity and p for the pressure of H_2. When $p = 1$ atm and the activity of H^+ ions is 1, the hydrogen electrode is called the standard hydrogen electrode (SHE) and its potential is zero by convention. The measured value of the potential difference of this cell is $+0.337$ V at 250°C. This measured cell potential difference, $+0.337$ V, is called the relative standard electrode potential of Cu and is denoted E^0. The standard electrode potential of other electrodes is obtained in a similar way, by forming a cell consisting of the SHE and the electrode under investigation. Standard electrode potentials at 25°C are listed in Table 1.1.

The potential E of the M^{z+}/M electrode is a function of the activity [see Eq. (1.5)] of metal ions in the solution according to the Nernst equation,

$$E = E^0 + \frac{RT}{zF} \ln a(M^{z+}) \tag{1.3}$$

TABLE 1.1 Standard Electrode Potentials

Metal/Metal Ion Couple	Electrode Reaction	Standard Value (V)
Au/Au^{+}	$Au^{+} + e \Leftrightarrow Au$	1.692
Au/Au^{3+}	$Au^{3+} + 3e \Leftrightarrow Au$	1.498
Pd/Pd^{2+}	$Pd^{2+} + 2e \Leftrightarrow Pd$	0.951
Cu/Cu^{+}	$Cu^{+} + e \Leftrightarrow Cu$	0.521
Cu/Cu^{2+}	$Cu^{2+} + 2e \Leftrightarrow Cu$	0.3419
Fe/Fe^{3+}	$Fe^{3+} + 3e \Leftrightarrow Fe$	−0.037
Pb/Pb^{2+}	$Pb^{2+} + 2e \Leftrightarrow Pb$	−0.1262
Ni/Ni^{2+}	$Ni^{2+} + 2e \Leftrightarrow Ni$	−0.257
Co/Co^{2+}	$Co^{2+} + 2e \Leftrightarrow Co$	−0.28
Fe/Fe^{2+}	$Fe^{1+} + 2e \Leftrightarrow Fe$	−0.447
Zn/Zn^{2+}	$Zn^{2+} + 2e \Leftrightarrow Zn$	−0.7618
$A1/A1^{3+}$	$Al^{3+} + 3e \Leftrightarrow Al$	−1.662
Na/Na^{+}	$Na^{+} + e \Leftrightarrow Na$	−2.71

Source: G. Millazzo and S. Caroli, *Tables of Standard Electrode Potentials*, Wiley, New York, 1978.

or converting the natural logarithm into the decimal logarithm yields

$$E = E^0 + 2.303\frac{RT}{zF}\ln a(M^{z+}) \tag{1.4}$$

where R, T, z, and F are the gas constant, absolute temperature, number of electrons involved in reaction (1.1a), and Faraday's constant (96,500 C), respectively. The activity of the ion, $a(M^{z+})$, is defined by

$$a(M^{z+}) = \gamma c(M^{z+}) \tag{1.5}$$

where $c(M^{z+})$ is the concentration of M^{z+} in moles per liter and $\gamma(M^{z+})$ is the activity coefficient of M^{z+}; when the concentration of a solution is low, such as 0.001 M or lower, the activity may be replaced by concentration in moles per liter.

The activity coefficient γ is a dimensionless quantity which depends on the concentration of all ions present in the solution (ionic strength). The individual activity coefficients of the specific ionic species cannot be measured experimentally, but it can be calculated. The experimentally measurable quantity is the mean total ionic activity $\gamma_{\pm}$:

$$\gamma_{\pm} = \sqrt{\gamma_{+}\gamma_{-}} \tag{1.6}$$

which is the geometric mean (the square root of the product) of the activity coefficients of the individual ionic species [2].

When the activity of M^{z+} in the solution is equal to 1, $a(M^{z+}) = 1$, then by Eqs. (1.3) and (1.4), since $\ln 1 = 0$,

$$E = E^0 \tag{1.7}$$

where E^0 is the relative standard electrode potential of the M^{z+}/M electrode. The quantity RT/F has the dimension of voltage and at 298 K (25°C) has the value of 0.0257 V and 2.303 $(RT/F) = 0.0592$ V. With these values Eq. (1.4) reads

$$E = E^0 + \frac{0.0592}{z}\log a(M^{z+}) \tag{1.8}$$

The use of Eq. (1.8) is illustrated in Examples 1.1 and 1.2.

Example 1.1 Calculate the reversible electrode potential of a Cu electrode immersed in a $CuSO_4$ aqueous solution with concentrations 1.0, 0.1, 0.01, and 0.001 mol L^{-1} at 25°C. The standard electrode potential for a Cu/Cu^{2+} electrode is 0.337 V. Use concentrations in Eq. (1.8) instead of activities in an approximate calculation.

From Eq. (1.8), for $z = 2$, $E^0 = 0.337$, and the concentration 1.0 mol L^{-1} solution, we obtain $E = 0.337 + (0.0592/2)$ $\log 1 = 0.337$ V, since $\log 1 = 0$. For the 0.1 mol L^{-1} solution, we obtain $E = 0.337 + (0.0592/2)\log\ 0.1 = 0.37$ V, since log 0.1 is −1. Using the same procedure for 0.01 and 0.001 mol L^{-1} solutions, we find that $E = 0.278$ and 0.248 V, respectively.

Example 1.2 Now calculate the reversible electrode potential of a Cu electrode for the conditions given in the Example 1.1, but use activities in Eq. (1.8) instead of concentrations. The mean activity coefficients of the above solutions, 1.0, 0.1, 0.01, and 0.001 are 0.043, 0.158, 0.387, and 0.700, respectively. Activities of these solutions are calculated using Eq. (1.5). For the 1.0 mol L^{-1} solution and $\gamma = 0.043$, we find that the activity of this solution is $a_{1.00} = \gamma c(Cu^{2+}) = 0.043 \times 1 = 0.043$. Activities for solutions 0.1,0.01, and 0.001 mol L^{-1} are 1.58×10^{-2}, 3.87×10^{-3}, and 7.00×10^{-4}, respectively.

Using Eq. (1.8) for the 1.00 mol L^{-1} solution, the reversible electrode potential at 25°C is $E = 0.337 + (0.0592/2)$ $\log\ 0.043 = 0.337 - 0.0400 = 0.297$ V. For 0.1, 0.01, and 0.001 mol L^{-1} solutions, the reversible electrode potentials at 25°C are 0.284, 0.266, and 0.244 V, respectively.

Hence Examples 1.1 and 1.2 illustrate that the effect of considering the activity coefficient in calculating electrode potential values is not substantial, and its effect decreases with a decrease in concentration, as seen in column 5 Table 1.2.

TABLE 1.2 Reversible Electrode Potential E of a Cu Electrode Immersed in a $CuSO_4$ Aqueous Solution

$CuSO_4$ Concentration, c (mol L^{-1})	E, V Calculated Using c	Activity, a	E, V Calculated Using a	ΔE, V
1.0	0.337	4.3×10^{-2}	0.297	0.040
0.1	0.307	1.58×10^{-2}	0.284	0.023
0.01	0.278	3.87×10^{-3}	0.266	0.012
0.001	0.248	7.00×10^{-4}	0.244	0.004

Note: See Example 1.2.

The difference ΔE in Table 1.2 is due to ion–ion interactions in the solution (1.1). The ion–ion interactions include interactions of the hydrated Cu^{2+} ions with one another and with SO_4^{2-} anions. In using concentration in Eq. (1.8) instead of activity, one thus neglects the ion–ion interactions.

In deposition of alloys it is frequently necessary to complex metal ions, as will be shown in Part B of this chapter. In this case the concentration or activity of metal ions in solution and the reversible electrode potential are calculated using the stability constant of the complex.

1.3 KINETICS AND MECHANISM OF ELECTRODEPOSITTON

1.3.1 Relationship between Current and Potential

When an electrode is made a part of an electrochemical cell through which current is flowing, its potential will differ from the equilibrium potential. If the equilibrium potential of the electrode (potential in the absence of current) is E and the potential of the same electrode as a result of current flowing is $E(I)$, then the difference η between these two potentials,

$$\eta = E(I) - E \tag{1.9}$$

is called *overpotential*.

An example of an electrochemical cell of industrial importance is shown in Figure 1.3. This figure shows how the potential $E(I)$ of a copper cathode in the etectrodeposition of copper can be measured using the three-electrode cell. The potential $E(I)$ of a Cu cathode, the test electrode, is measured versus a reference electrode (e.g., saturated calomel electrode), a Lugin capillary, and a high-input-impedance device (voltmeter) so that a negligible current is drawn through the reference electrode.

For large negative values of overpotentials ($\eta \geq 100$ mV) the current density i ($i = I/S$, where S is the surface area of the electrode) increases exponentially with the overpotential η according to the equation

$$i = -i_0 e^{-\alpha z f \eta} \tag{1.10}$$

and for large positive values of overpotential (anodic processes) according to the equation

$$i = -i_0 e^{(1-\alpha) z f \eta} \tag{1.11}$$

where i_0 is the exchange current density ($i_0 = i$ when $\eta = 0$), α the transfer coefficient, F the Faraday constant, R the gas constant, T the absolute temperature, and

$$f = \frac{F}{RT} \tag{1.12}$$

From Eqs. (1.10) and (1.11) it follows that, for $\eta = 0$, $i = i_0$ Thus, when an electrode is at equilibrium, there is a constant exchange of charge carriers (electrons or ions) across the metal–solution interphase (Eq. 1.1b).

At 25°C,

$$f = \frac{96487\ \text{C mol}^{-1}}{8.3144\ \text{J K}^{-1}\ \text{mol}^{-1} \times 298\ \text{K}} = 38.94\ \text{V} \tag{1.13}$$

since the Faraday constant $F = 96{,}487.0\ \text{C mol}^{-1}$, the gas constant $R = 8.3144\ \text{J mol}^{-1}\ \text{deg K}^{-1}$, and joules = volts × coulombs. These exponential relationships show that even small changes in η produce large changes in the current density, as seen from Figure 1.4. Taking the logarithm of Eqs. (1.10) and (1.11) and solving the resulting equations for η, one obtains the Tafel equation:

$$\eta = a \pm b \log|i| \tag{1.14}$$

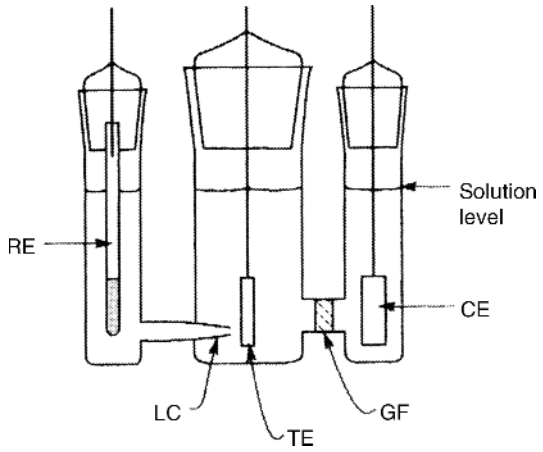

FIGURE 1.3 Three-component, three-electrode electrochemical cell: RE, reference electrode; LC, Lugin capilary; TE, test electrode; GF, glass frit; CE, counterelectrode.

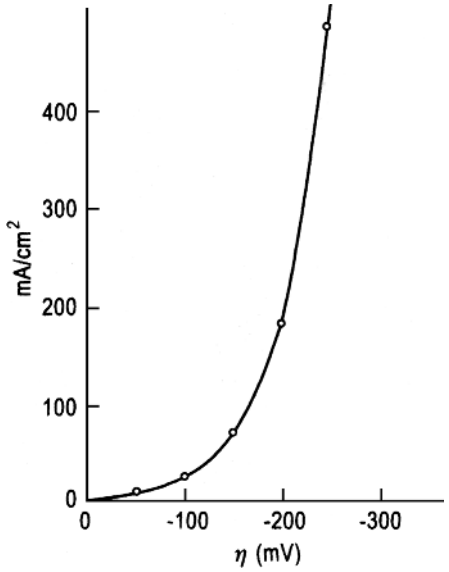

FIGURE 1.4 Exponential relationship between current density and overpotential for electrodeposition of copper from an aqueous solution of 0.15 N $CuSO_4$ and 1.0 N H_2SO_4.

where a and b are constants and $|i|$ is the absolute value of the current density. The $\pm$ sign holds for anodic and cathodic processes, respectively. The theoretical value of the constant a for the cathodic process (a_c), is

$$a_c = \frac{2.303RT}{\alpha zF} \log i_0 \tag{1.15}$$

and that of b_c is

$$b_c = \frac{2.303RT}{\alpha zF} \tag{1.16}$$

The use of Eqs. (1.10) and (1.14) is illustrated in Examples 1.3 and 1.4.

Example 1.3 Mattsson and Bockris [3] studied the electrodeposition of copper from the aqueous solution 0.15 N $CuSO_4$ and 1.0 N H_2SO_4 and determined that the exchange current density for this process is 3.7 mA cn^{-2} (3.7×10^{-3} A cm^{-2}). Using Eq. (1.10), we calculate the cathodic current densities i as a function of overpotential value of -50, -100, -150, -200, and -250 mV. For α we take the most frequent value, $\alpha = 0.5$, and for temperature, 25°C. Next we plot $i = f(\eta)$.

Using Eq. (1.10), we see that i (in A cm^{-2}) for $\eta = -50$ mV (-0.050 V) is

$$i = -i_0 e^{-\alpha f \eta} = (-3.7 \times 10^{-3}) e^{0.9737} = -9.80 \times 10^{-3}\,\text{A cm}^{-2}$$

since we have $-\alpha f \eta = -0.5 \times 38.94 \times (-0.050) = 0.9737$ and $e = 2.7183$. For $\eta = -100$ mV(0.100 V),

$$i = -i_0 e^{-\alpha f \eta} = (-3.7 \times 10^{-3}) e^{1.947} = -25.9 \times 10^{-3}\,\text{Acm}^{-2}$$

since we now have $-\alpha f \eta = -0.5 \times 38.94 \times (-0.100) = 1.947$.

In the same way we find i for the other η values. These are shown in Table 1.3.

The calculated values of η are used to plot the $i = f(\eta)$ function corresponding to this example Fig. 1.4. It again illustrates that even small increases in η result in large changes in the current density i.

TABLE 1.3 Current and Overpotential for Electrodeposition of Copper from Add Copper Sulfate Solution

Overpotential $-\eta$ (mV)	Current Density, i (mA cm^{-2})	log i
50	9.80	0.991
100	25.9	1.41
150	68.7	1.84
200	182	2.26

Note: See Example 1.3.

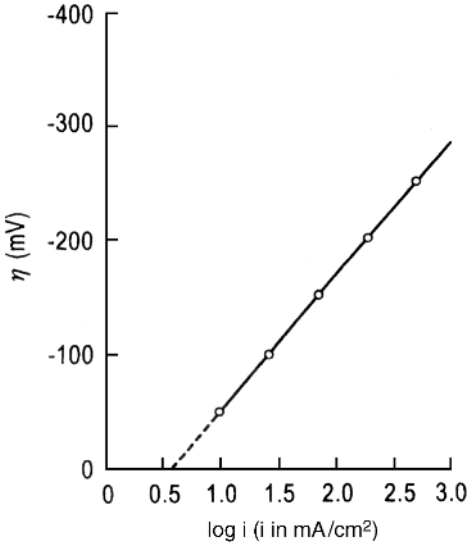

FIGURE 1.5 Tafel plot, $\eta = f(\log i)$, for electrodeposition of copper from the aqueous solution of 0.15 N $CuSO_4$ and 1.0 N H_2SO_4.

Example 1.4 Using the calculated values of i for the given values of η from Table 1.3 plot the corresponding Tafel equation, $\eta = f$ (log i).

The solution is given in Figure 1.5. It shows that for large values of $\eta (\eta \geq 100\,\text{mV})$ the function $\eta = f$ (log i) is a straight line. The experimentally determined cathodic and anodic Tafel lines for electrodeposition of copper in acid copper sulfate solution are shown in Figure 1.6. The figure shows that the transfer coefficients for the anodic and cathodic processes are different and that the extrapolated value of i at $\eta = 0$ gives the exchange currenty density. The transfer coefficient α_c for the cathodic process (deposition of Cu^{2+}) is obtained from the slope $d\eta/d(\log i)$ of the cathodic Tafel line. That for the anodic process, α_a, is obtained from the slope of the Tafel line for the anodic process.

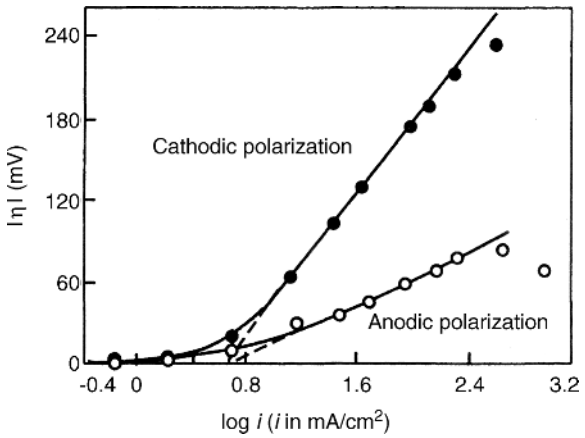

FIGURE 1.6 Current–potential relationship for the electrodeposition of copper from an acid $CuSO_4$ solution. (From J. O'M. Bockris, in *Transactions of the Symposium on Electrode Processes*, E. Yeager, Ed., Wiley, New York, 1961, with permission from the Electrochemical Society.)

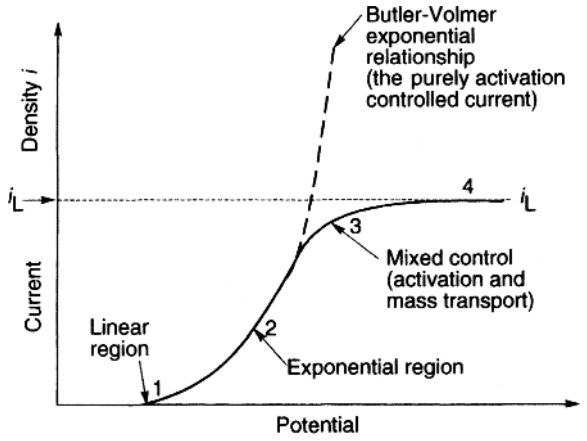

FIGURE 1.7 Four regions in the general current–overpotential relationship: 1, linear; 2, exponential; 3, mixed control; 4, limiting current density region.

1.3.2 Influence of Mass Transport on Electrode Kinetics

The current–potential relationship defined by Eqs. (1.10, 1.11) and (1.14) is valid for the case where the charge transfer, Eq. (1.1), is the slow process (rate-determining step). This relationship has a limit where the rate of deposition reaction is limited by transport of M^{z+} ions. A general current–potential relationship is shown in Figure 1.7. The limiting, or maximum, current density is given by [4]

$$i_L = \frac{nFD}{\delta} c_b \tag{1.17}$$

where D is the diffusion coefficient of the depositing species M^{z+}, c_b is the bulk concentration of M^{z+} ions in the solution, δ is the diffusion layer thickness, n the number of electrons involved in the reaction, and F the Faraday constant. The diffusion layer thickness δ is defined by the Nernst diffusion layer model illustrated in Figure 1.8. This model assumes that the concentration of M^{z+} ions has a bulk concentration c_b up to a distance δ from the electrode surface and then falls off linearly to $c_{x=0}$ at the electrode surface. In this model it is assumed that the liquid layer of thickness δ is practically stationary (quiescent). At a distance greater than δ from the surface, the concentration of the reactant M^{z+} is assumed to be equal to that in the bulk. At these distances, $x > \delta$, stirring is efficient. Ions M^{z+} must diffuse through the diffusion layer to reach the electrode surface.

At the values of the limiting (maximum) current density the species M^{z+} are reduced as soon as they reach the electrode. At these conditions the concentration of the reactant M^{z+} at the electrode is nil, and the rate of deposition reaction is controlled by the rate of transport of the reactant M^{z+} to the electrode. If an external current greater than the limiting current i_L is forced through the electrode, the double

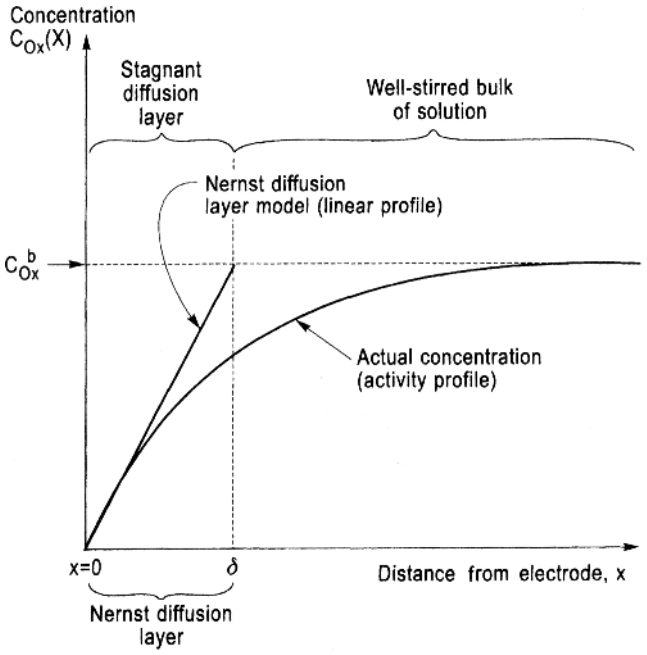

FIGURE 1.8 Variation of the concentration of the reactant during non-steady-state electrolysis; c^b_{Ox} is the concentration in the bulk; $c_{Ox}(x)$ is the concentration at the surface.

layer is further charged, and the potential of the electrode will change until some other process, other than reduction of M^{z+}, can occur. It will be shown later that the limiting current density is of great practical importance in metal deposition since the type and quality of metal deposits depend on the relative values of the deposition current and the limiting current. One extreme example is shown in Figure 1.9.

Example 1.5 Calculate the diffusion limiting current density i_L for the deposition of a metal ion M^{2+} at a cathode in a quiescent (unstirred) solution assuming the diffusion

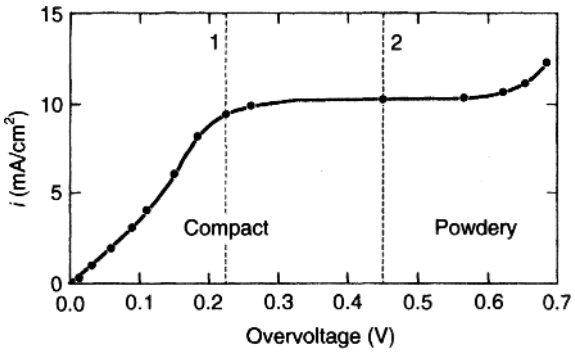

FIGURE 1.9 Overpotential characteristic of transition from compact to powdery deposit in electrodeposition of Cu from $CuSO_4$ (0.1 M) + H_2SO_4 (0.5 M) solution. (From N. Ibl, in *Advances in Electrochemistry and Electrochemical Engineering*, Vol. 2, C. W. Tobias, Ed., Wiley, New York, 1962, with permission from Wiley.)

layer thickness δ is 0.05 cm. The concentration of M^{2+} ions in the bulk (c_b) is 10^{-2} mol L^{-1} (10^{-5} mol cm^{-3}) and the diffusion coefficient D of M^{2+}, in the unstirred solution, is 2×10^{-5} cm^2 s^{-1}.

Using Eq. (1.17), we calculate that the limiting diffusion current density for this case is

$$i_L = \frac{nFD}{\delta} c_b = \frac{2 \times 96487 \times 2 \times 10^{-5} \times 10^{-5}}{0.05}$$
$$= 7.72 \times 10^{-4} \text{ A cm}^{-2} = 0.72 \text{ mA cm}^{-2}$$

In the same way we find that, for $c_b = 10^{-1}$ mol L^{-1} (10^{-4} mol cm^{-3}), $i_L = 7.20$ mA cm^{-2}.

In the stirred electrolyte solution the diffusion layer thickness δ and the limiting current density i_L depend on the nature of stirring.

For a rotating electrode the diffusion layer thickness depends on the angular speed of rotation ω according to

$$\delta = \frac{1.61 D^{1/6} \nu^{1/6}}{\sqrt{\omega}} \tag{1.18}$$

and the limiting current density depends on ω according to

$$i_L = \frac{0.62 nFaD^{2/3} c}{\nu^{1/6}} \sqrt{\omega} \tag{1.19}$$

where D is the diffusion coefficient, ν the kinematic viscosity (the coefficient of viscosity/density of the liquid), ω the rotation angular speed (in radians per second), c the concentration of the solution, and a the disc surface area [4]. We use these equations in the next two examples.

Example 1.6 Determine the diffusion layer thickness for a rotating electrode at 60, 240, and 360 rpm. For kinematic viscosity ν use 10^{-2} cm^2 s^{-1} and for the diffusion coefficient D use 10^{-5} cm^2 s^{-1}.

For the above given values for ν and D, Eq. (1.18) becomes

$$\delta = \frac{1.61 \times 10^{-2}}{\sqrt{\omega}} = \frac{1.61 \times 10^{-2}}{\sqrt{2\pi N}}$$

In the above equation the rotation speed w in radians per second is replaced by $\omega = 2\pi N$, where N is the number of rotations per second, rps.

Applying the above equation for $N = 1$ rps (60 rpm), one gets $\delta = 64$ μm. For $N = 4$ rps (240 rpm), $\delta = 32$ μm, and for $N = 6$ rps (360 rpm), $\delta = 26$ μm.

Example 1.7 Calculate the limiting current density i_L for the deposition of a metal ion M^{2+} at a rotating disc cathode with a surface area $a = 1$ cm^2 and the rotating speed 300 rpm (5 rps) using Eq. (1.19) assuming that the concentration of M^{2+} is 10^{-5} mol cm^{-3} (10^{-2} mol L^{-1}). The diffusion coefficient D of M^{2+} is 2×10^{-5} cm^2, $\nu = 10^{-5}$ cm^2 s^{-1}.

Substitution of the above given values for a, D, and ν into Eq. (1.19) yields

$$i_L = (1.91 \times 10^2) c \sqrt{\omega}$$

For $c = 10^{-2}$ mol $L^{-1} = 10^{-5}$ mol cm^{-3} and $\omega = 2\pi N = 31.41$

$$i_L = 1.07 \times 10^{-2} \text{ A cm}^{-2} = 10.7 \text{ mA cm}^{-2}$$

This value should be compared with the i_L value for a quiescent (unstirred) solution in Example 1.5.

1.3.3 Faraday's Law

Faraday's law states that the amount of electrochemical reaction that occurs at an electrode is proportional to the quantity of electric charge Q passed through an electrochemical cell. Thus, if the weight of a product of electrolysis is w, then Faraday's law states that

$$w = ZQ \tag{1.20}$$

where Z is *the electrochemical equivalent*, the constant of proportionality. Since Q is the product of the current I in amperes and the elapsed time t in seconds,

$$Q = It \tag{1.21}$$

$$w = ZIt \tag{1.22}$$

According to Faraday's law the production of one gram equivalent of a product at the electrode, W_{eq}, in a cell requires 96,487 C. The constant 96,487 is termed the Faraday *constant F*. The coulomb (C) is the quantity of electricity transported by the flow of one ampere for one second.

The Faraday constant represents one mole of electrons and its value can be calculated from

$$F = N_A e \tag{1.23}$$

where N_A is Avogadro's number (6.0225×10^{23} molecules mol^{-1}) and e is the charge of a single electron (1.6021×10^{-19} C):

$$F = (6.0225 \times 10^{23})(1.6021 \times 10^{-19}) = 96,487 \text{ C mol}^{-1} \tag{1.24}$$

One equivalent, w_{eq}, is that fraction of a molar (atomic) unit of reaction that corresponds to the transfer of one electron. For example, w_{eq} for silver is the gram atomic

weight of silver, since the reduction of Ag^+ requires one electron. The deposition of copper from a Cu^{2+} salt involves two electrons, and the w_{eq} for Cu is (gram atomic weight of Cu)/2. In general,

$$w_{eq} = \frac{A_{wt}}{n} \tag{1.25}$$

where A_{wt} is the atomic weight of metal deposited on the cathode and n the number of electrons involved in the deposition reaction.

From Eqs. (1.20) and (1.22) it follows that when $Q = 1$ C, or $Q = 1$ A s, then

$$w_{Q=1} = Z \tag{1.26}$$

Thus the electrochemical equivalent of a metal M, Z(M), is the weight in grams produced, or consumed, by one coulomb (one ampere second). The combination of Eqs. (1.20) and (1.26) yields

$$w = w_{Q=1}Q \tag{1.27}$$

The value of Z, or $w_{Q=1}$, can be evaluated in the following way. Since 96,487 C is required for the deposition of an equivalent of a metal, w_{eq}, from Eq. (1.20) it follows that

$$w_{eq} = 96,487Z \tag{1.28}$$

and

$$Z = w_{Q=1} = \frac{w_{eq}}{96,487} = \frac{w_{eq}}{F} \tag{1.29}$$

Since $w_{eq} = A_{wt}/n$ [Eq. (1.25)],

$$Z = \frac{A_{wt}}{nF} \tag{1.30}$$

Finally, from Eqs. (1.20) and (1.30)

$$w = ZQ = \frac{A_{wt}}{nF}Q \tag{1.31}$$

Example 1.8 Determine the electrochemical equivalent of Cu for the case of electrodeposition of Cu from Cu^{2+} solutions. The atomic weight of Cu is 63.55.

From Eq. (1.29),

$$Z(Cu^{2+}) = \frac{A_{wt}Cu}{nF} = \frac{63.55}{2 \times 96,487} = 3.293 \times 10^{-4}\ gC^{-1}$$

Example 1.9 A current of 300 mA was passed for 20 min through an electrochemical cell containing copper electrodes in H_2SO_4 acidified $CuSO_4$ aqueous solution. Calculate the amount of copper deposited at the cathode. The gram atomic weight of Cu is 63.55.

In order to calculate w using Eq. (1.31), we find first the number of coulombs Q, the quantity of electricity passed during the electrolysis,

$$Q = It = 0.300A \times 1200\ s = 360\ As = 360\ C$$

The number of electrons n involved in the Cu deposition reaction

$$Cu^{2+} + 2e = Cu$$

is 2. Substituting these values into Eq. (1.31), we get the amount of Cu deposited at the electrode,

$$w = \frac{63.55 \times 360}{2 \times 96,487} = 0.118g$$

Alternatively, using the value of the electrochemical equivalent for Cu, $Z(Cu^{2+}) = 3.293 \times 10^{-4}$ g C^{-1}, and Eq. (1.31), we get

$$w = ZQ = 3.293 \times 10^{-4} \times 0.300 \times 1200 = 0.118g$$

1.3.4 Current Efficiency

When two or more reactions occur simultaneously at an electrode, the number of coulombs of electricity passed corresponds to the sum of the number of equivalents of each reaction. For example, during deposition of Cu from a solution of cupric nitrate in dilute nitric acid, three cathodic reactions occur: the deposition of Cu (the reduction of cupric ions) and the reduction of both nitrate and hydrogen ions.

The current efficiency CE of the jth process, namely of any one of the simultaneous reactions, is defined as the number of coulombs required for that reaction, Q_j, divided by the total number of coulombs passed, Q_{total}:

$$CE = \frac{Q_j}{Q_{total}} \tag{1.32}$$

An alternative equation defining current efficiency is

$$CE = \frac{w_j}{w_{total}} \tag{1.33}$$

where w_j is the weight of metal j actually deposited and w_{total} is that which would have been deposited if all the current had been used for depositing metal j.

Thus, in general, at a current efficiency under 100%, the remainder of the current is used in side processes, such as the reduction of hydrogen and nitrate ions in the example above.

Example 1.10 When a current of 3 A flows for 8 min through a cell composed of two Pt electrodes in a solution of $Cu(NO_3)_2$ in dilute HNO_3 acid, 0.36 g of Cu is deposited on the cathode. Calculate the current efficiency for the deposition of copper.

The number of coulombs required for deposition of 0.36 g of Cu is obtained from Eq. (1.31):

$$Q_j = \frac{wn \times 96,487}{A_{wt}} = \frac{0.36 \times 2 \times 96,487}{63.55} = 1093$$

$$Q_{total} = It = 3 \times 480 = 1440$$

and

$$\text{CE} = \frac{Q_j}{Q_{total}} = \frac{1093}{1440} = 0.759 \text{ or CE} = 75.9\%$$

1.3.5 Deposit Thickness

The deposit thickness may be evaluated by considering the volume of the deposit. Since the volume of the deposit V is the product of the plated surface area a and the thickness (height) h, it follows that $h = V/a$. The volume of the deposit is related to the weight of the deposit w and the density of the deposit d by the relationship defining the density, $d = w/V$. Thus

$$h = \frac{V}{a} = \frac{w}{ad} \tag{1.34}$$

In the case where it is necessary to calculate the time t (in seconds) required to obtain the desired deposit thickness h at a given current density, we introduce Faraday's law [Eq. (1.31)], into Eq. (1.34) and obtain

$$h = \frac{w}{ad} = \frac{ZQ}{ad} = \frac{ZIt}{ad} \text{ cm} \tag{1.35}$$

$$t = \frac{had}{ZI} \text{ s} \tag{1.36}$$

Example 1.11 The weight of a Co deposit is 0.00208 g on a substrate with surface area of 7.5 cm^2. What is the thickness of the Co deposit. Remember that the density of Co is 8.71 g cm^{-3}.

Using Eq. (1.34), we have that

$$h = \frac{0.00208}{7.5 \times 8.71} = 3.184 \times 10^{-5} \text{ cm} = 3184\text{Å}$$

Example 1.12 Determine the time required to obtain a Cu deposit of thickness 1 μm (10^{-4}cm) when electrodeposition is done at 4 and 6 A. The surface area a of the substrate is 314 cm^2.

From Eq. (1.36), for $I = 4$A,

$$t = \frac{had}{ZI} = \frac{10^{-4} \times 314 \times 8.93}{3.29 \times 10^{-4} \times 4} = 213 \text{ s} = 3 \text{ min}, 33 \text{ s}$$

for $I = 6$A, in the same way, one obtains that $t = 142$ s = 2 min, 22 s.

1.3.6 Atomistic Aspects of Electrodeposition

In the electrodeposition of metals, generally a metal ion M^{z+} is transferred from the solution into the ionic metal lattice. A simplified atomistic representation of this process is

$$M^{z+}(\text{solution}) \rightarrow M^{z+}(\text{lattice}) \tag{1.37}$$

This reaction is accompanied by the transfer of z electrons from an external electron source (e.g., power supply) to the electron gas in the metal M.

Before discussing the individual atomistic processes that make up the overall electrodeposition process, [Eq. (1.37)], it is necessary to consider the basic characteristics of the bulk and the surface structures of metals [1]. A metal may be considered to be a fixed lattice of positive ions permeated by a gas of free electrons. Positive ions are the atomic cores, while the negative charges are the valence electrons. For example, the copper atom has a configuration (electronic structure) $1s^2 2s^2 2p^6 3s^2 3p^6 3d^{10} 4s^1$ (the superscripts indicate the number of electrons in the orbitconfiguration) with a single valence electron (4s). The atomic core of Cu^+ has the set of configurations given above less the one valence electron $4s^1$. The free electrons form what is known as the *electron gas* in the metal, and they move nearly freely through the volume of the metal. Each metal atom thus contributes its single valence electron to the electron gas in the metal. Interactions between the free electrons and the metal ions are largely responsible for the metallic bond.

Surfaces may be divided into ideal and real. Ideal surfaces exhibit no surface lattice defects (vacancies, impurities, grain boundaries, dislocations, etc.). Real surfaces have a variety of defects. For example, the density of metal surface atoms is about $10^{15} cm^{-2}$, while the density of dislocations is of the order of $10^8 cm^{-2}$. The structure of real surfaces differs from those of ideal surfaces by surface roughness. While an ideal surface is atomically smooth, a real surface may have defects, steps, kinks, vacancies, and clusters of adatoms (Fig. 1.10).

The atomic processes that make up the electrodeposition process [Eq. (1.37)] can be viewed considering the structure of the initial, M^{z+} (solution), and the final state, M^{z+} (lattice). Since metal ions in an aqueous solution are hydrated, the structure of the initial state in Eq. (1.37) should be

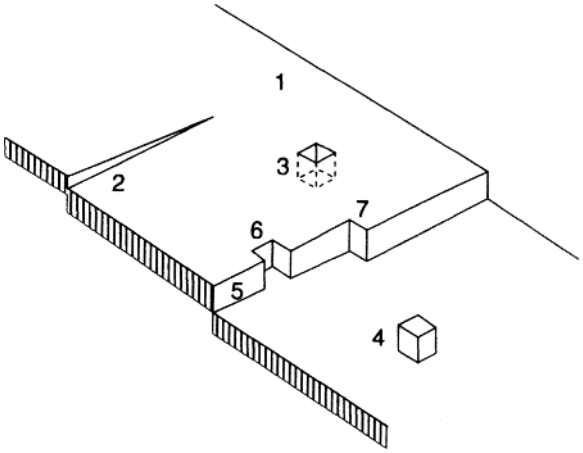

FIGURE 1.10 Some simple defects found on a low-index crystal face: 1, perfect flat face, terrace; 2, an emerging screw dislocation; 3, a vacancy in the terrace; 4, an adatom on the terrace; 5, a monatomic step in the surface, a ledge; 6, a vacancy in the ledge; 7, a kink, a step in the ledge.

represented by $[M(H_2O)_x]^{z+}$. The structure of the final state is an M adion (adatom; adsorbed ion, atom) at a kink site (Fig. 1.11), since it is generally assumed that atoms (ions) are attached to a crystal via a kink site [1]. Thus the final step of the overall reaction [Eq. (1.37)] is the incorporation of the M^{z+} adion into the kink site. Because of surface inhomogeneity, the transition from the initial state $[M(H_2O_x)]^{z-}$ (solution) to the final state M^{z+} (kink),

$$[M(H_2O)_x]^{z+}\,(\text{solution}) \rightarrow M^{z+}\,(\text{kink}) \qquad (1.38)$$

may proceed via either of the two mechanisms: (1) step-edge site ion transfer or (2) terrace site ion transfer.

Step-Edge Ion-Transfer Mechanism The step-edge site ion transfer, or direct transfer mechanism, is illustrated in Figure 1.12. As the figure shows, this mechanism ion transfer from the solution takes place on a kink site of a step edge or on any other site on the step edge. In both cases the result of

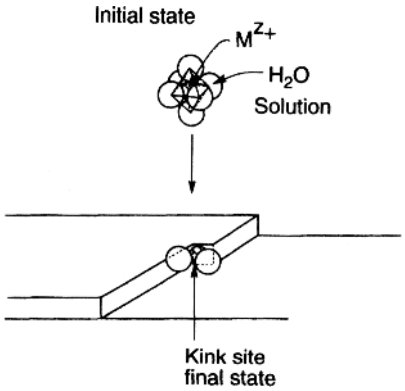

FIGURE 1.11 Initial and final states in metal deposition.

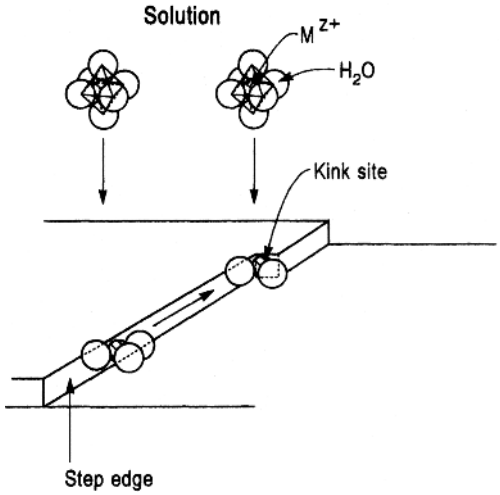

FIGURE 1.12 Step-edge ion-transfer mechanism.

the ion transfer is an M adion in the metal crystal lattice. In the first case of a direct transfer to the kink site, the M adion is in the half-crystal position, where it is bonded to the crystal lattice with one-half of the bonding energy of the bulk ion. Thus the M adion belongs to the bulk crystal. However, it still has some water of hydration (Fig. 1.12). In the second case of a direct transfer to the step-edge site other than a kink, the transferred metal ion diffuses along the step edge until it finds a kink site (Fig. 1.12). Thus, in a step-edge site transfer mechanism, there are two possible paths: direct transfer to a kink site and the step-edge diffusion path.

Terrace Ion-Transfer Mechanism In the terrace site transfer mechanism a metal ion is transferred from the solution to the flat face of the terrace region (Fig. 1.13). At this position the metal ion is in the adion (adsorbedlike) state having most of the water of hydration. It is weakly bound to the crystal lattice. From this position it diffuses on the surface, seeking a position of lower energy. The final position is a kink site.

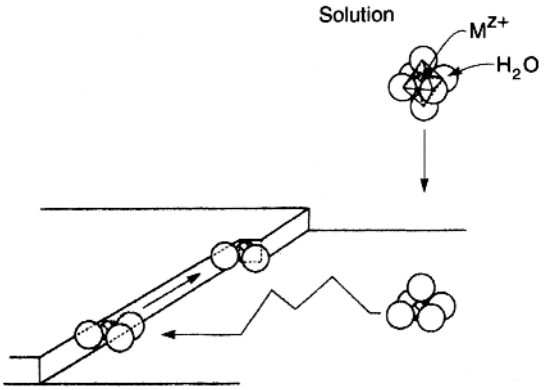

FIGURE 1.13 Ion transfer to a terrace site, surface diffusion, and incorporation at kink site.

In view of these two mechanisms—the step edge and terrace ion transfer—the overall current density i is considered to be composed of two components:

$$i = i_{se} + i_{te} \tag{1.39}$$

where i_{se} and i_{te} are the step-edge and terrace site current density components, respectively.

The initial theoretical treatment of these mechanisms of deposition was given by Lorenz [5–8], The initial experimental studies on surface diffusion were published by Mehl and Bockris [9, 10]. Conway and Bockris [11, 12] calculated the activation energies for the ion-transfer process at various surface sites, Simulation of crystal growth via surface diffusion was discussed by Gilmer and Bennema [13].

1.3.7 Pulse Deposition Techniques

One important effect in pulse deposition techniques is a modification of the diffusion layer [14]. The Nernst diffusion layer model is illustrated in Figure 1.8 and described in Section 1.3.2. Under pulse deposition conditions the Nernst diffusion layer is split into two diffusion layers, as is schematically shown in Figure 1.14. In the pulsating diffusion layer, which is in the immediate vicinity of the cathode, the metal ion concentration pulsates with the frequency of the pulsating current [14]. Pulse deposition techniques are used mostly to improve the distribution of the deposit (current distribution), the leveling, and the brightness of the deposit [15].

The four major waveforms that are used in pulse deposition techniques are shown in Figure 1.15. In the *rectangular-pulse deposition* technique the waveform consists of pulses of a current or potential of a rectangular shape separated by intervals of zero current or potential. The shape of this waveform is shown in Figure 1.15*a*. where I or E is

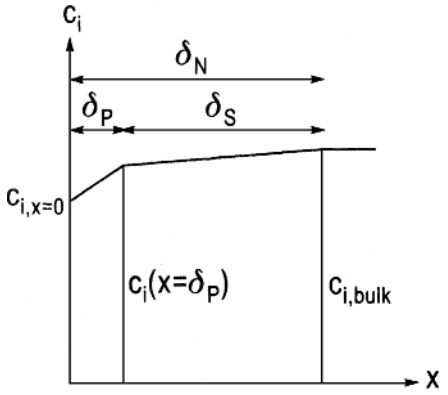

FIGURE 1.14 Schematic concentration profile at the cathode for pulse plating conditions: δ_p, pulsating diffusion layer thickness; δ_s, stationary diffusion layer thickness; δ_N, Nernst diffusion layer thickness.

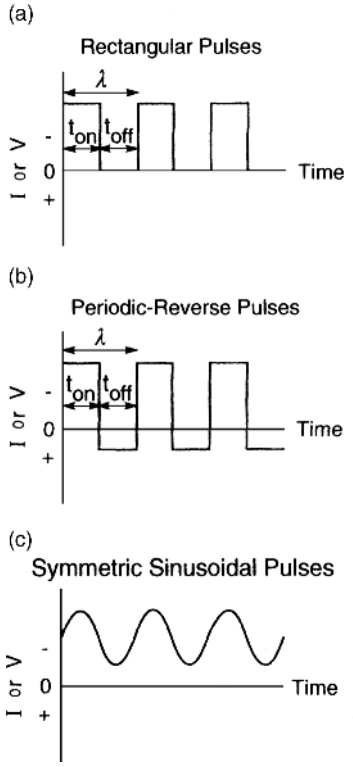

FIGURE 1.15 Three major waveforms used in pulse deposition: t_{on}, the on period of a pulse; t_{off}, the off period; λ, the cycle time; t_c, the cathodic pulse period; t_a, the anodic pulse period.

the maguitude of the applied current or potential, t_{on} is the on period of a pulse, t_{off} is the off period, and λ is the cycle time. The waveform of *periodic reverse deposition* is shown in Figure 1.15*b*. It is seen that in this technique the applied current or potential is periodically switched from cathodic to anodic polarization; t_c is the cathodic pulse period, t_a the anodic pulse period, and λ the cycle time.

A *superimposed sinusoidal deposition* waveform is shown in Figure 1.15*c*. This waveform is the sum of a sinusoidal alternating (ac) wave, current or potential, and a direct cathodic current (dc). If the amplitude of the sine wave is greater than the dc offset, then the waveform consists of both a cathodic and an anodic portion.

There is now increased interest in pulse deposition techniques because of recently published data on the beneficial use of pulse plating in the fabrication process of integrated circuits [16].

1.4 GROWTH MECHANISM

There are two basic mechanisms for formation of a coherent deposit [1, 17]: layer growth and three-dimensional (3D) crystallite growth (or nucleation–coalescence growth). A schematic illustration of these two mechanisms is given in Figure 1.16.

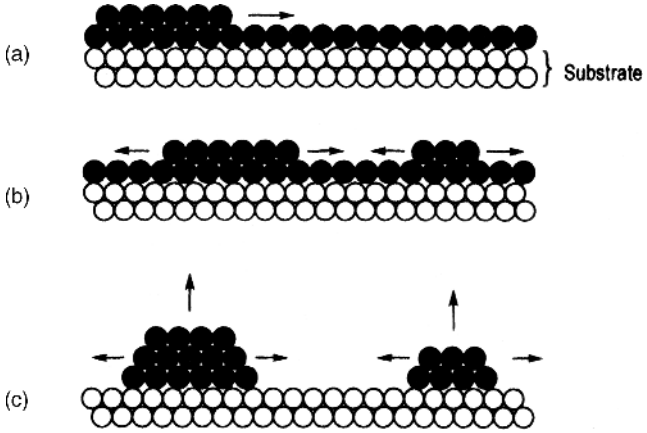

FIGURE 1.16 Schematic representation of layer growth (*a, b*) and the nucleation–coalescence mechanism (*c*).

In the layer growth mechanism a crystal enlarges by a spreading of discrete layers (steps), one after another across the surface. In this case a growth layer, a step, is a structure component of a coherent deposit. Steps, or growth layers, are the structural components for the construction of a variety of growth forms in the electro-deposition of metals (e.g., columnar crystals, whiskers, and fiber texture). We can distinguish among monoatomic steps, polyatomic microsteps, and polyatomic macrosteps. In general, there is a tendency for a large number of thin steps to bunch into a system of a few thick steps. Many monoatomic steps can unite (bunch, coalesce) to form a polyatomic step.

In the 3D crystallite growth mechanism the structural components are 3D crystallites, and a coherent deposit is built up as a result of coalescence (joining) of these crystallites. The growth sequence of electrodeposition via nucleation–coalescence consists of four stages: (1) formation of isolated nuclei and their growth to TDC (three dimensional crystallites), (2) coalescence of TDC, (3) formation of linked network, and (4) formation of a continuous deposit.

Development of Columnar Microstructure The columnar microstructure is perpendicular to the substrate surface, as shown schematically in Figure 1.17. This microstructure is composed of relatively fine grains near the substrate but then changes to a columnar microstructure with much coarser grains at greater distances from the substrate. The development of the columnar microstructure may be interpreted as the result of growth competition among adjacent grains. The low-surface-energy grains grow faster than the high-energy ones. This rapid growth of the low-surface-energy grains at the expense of the high-energy grains results in an increase in mean grain size with increased thickness of deposit and the transition from a fine grain size near the substrate to a coarse, columnar grain size [1, 18].

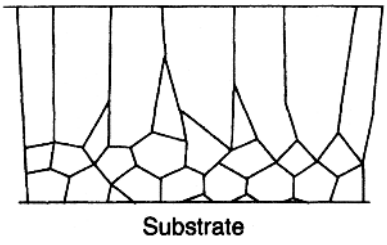

FIGURE 1.17 Schematic cross section (perpendicular to the substrate) of the columnar deposit.

Overpotential Dependence of Growth Forms The development of growth forms on overpotentials stems from the potential dependence of the nucleation and growth processes. Competition between nucleation and growth processes is strongly influenced by the potential of the cathode [1, 19].

1.4.1 Effect of Additives

Additives affect deposition and crystal-building processes as adsorbates (adsorbed substances) at the surface of the cathode. There are two basic types of adsorption: chemisorption (an abreviation of *chemical adsorption*) and physisorption (an abreviation of *physical adsorption*). In chemisorption the chemical attractive forces of adsorption act between the surface and the absorbate (usually these are covalent bonds). Thus there is a chemical combination between the substrate and the adsorbate where electrons are shared and/or transferred. New electronic configurations may be formed through this sharing of electrons. In physisorption the physical forces of adsorption, van der Waals or electrostatic forces, act between the surface and the adsorbate; there is no electron transfer and no electron sharing.

The adsorption energy for chemisorbed species is greater than that for physisorbed species. Typical values for chemisorption are in the range of 20–100 kcal mol^{-1} and for physisorption, around 5 kcal mol^{-1}.

1.4.2 Effect of Additives on Nudeation and Growth

Adsorbed additives affect the kinetics of electrodeposition and the growth mechanism by changing the concentration of growth sites on a surface, the concentration of adions on the surface, the diffusion coefficient D, and the activation energy of surface diffusion of adions. In the presence of adsorbed additives the mean free path for lateral diffusion of adions is diminished, which is equivalent to a decrease in the diffusion coefficient D (diffusivity) of adions. This decrease in D may result in an increase in adion concentration at steady state and thus an increase in the frequency of the two-dimensional nucleation between diffusing adions.

Additives can also influence the propagation of microsteps and cause bunching and the formation of macrosteps.

The type of deposit obtained at constant current density may depend on the surface coverage of additives.

1.4.3 Leveling

Leveling is defined as the progressive reduction of the surface roughness during deposition. Surface roughness may be the result of mechanical polishing. In this case scratches on the cathode represent the initial roughness and the result of cathodic leveling is a smooth (flat) deposit or a deposit of reduced roughness. During this type of leveling more metal is deposited in recessed areas than on peaks (bumps). This leveling is of great value in the metal-finishing industry. Leveling can be achieved in solutions either in the absence of addition agents or in the presence of leveling agents. Thus there are two types of leveling processes: (1) geometric leveling corresponding to leveling in the absence of specific agents and (2) true or electrochemical leveling corresponding to leveling in the presence of leveling agents.

Dukovic and Tobias [20] and Madore and Landolt [21] developed theoretical models of leveling during electrodeposition in both the absence and presence of additives. Both models indicate that a significant leveling of semicircular and triangular grooves by uniform current distribution (geometric leveling) is achieved when the thickness of deposit is at least equal to to the depth of the groove. Leveling in the presence of leveling agents (true leveling) is achieved at much lower deposit thickness.

Theories of leveling by additives are based on (1) the correlation between an increase in the polarization produced by the leveling agents [22] and (2) preferential adsorption of a leveling agent on the high point (peaks of the substrate or flat surfaces) and by this inhibition (slowing down) of deposition at these points [1, 23].

1.4.4 Brightening

The brightness of a surface is defined as the optical reflecting power of the surface. It is measured by the amount of light specularly reflected (Fig. 1.18). Weil and Paquin [24] showed a linear relationship between the logarithm of the amount of light specularly reflected by a surface and the fraction of the surface having roughness of less than 1500 Å. Kardos and Foulke [23] distinguish three possible mechanisms for bright deposition: (1) diffusion-controlled leveling, (2) grain refining, and (3) randomization of crystal growth. Some fundamental aspects of brightening and leveling are reviewed by Oniciu and Muresan [25].

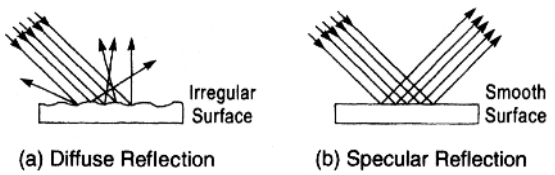

FIGURE 1.18 Diffuse and specular reflection. The surface of the object that has irregularities diverges out an initially parallel beam of light in all directions to produce diffusion reflection (*a*). A smooth, bright surface specularly reflects a parralel beam of light in one direction only (*b*).

1.4.5 Consumption of Additives

An additive can be consumed at the cathode by incorporation into the deposit and/or by the electrochemical reaction at the cathode or anode. Consumption of coumarin in the deposition of nickel from the Watts-type solution was studied extensively. For example, Rogers and Taylor [26] found that the coumarin concentration decreases linearly with time and that the rate of coumarin consumption is a function of concentration. The rate of consumption increases with increase in the bulk concentration of the coumarin. Thus, in the electrodeposition of nickel from a Watts-type solution, the total current density is the sum of the current densities for nickel deposition, hydrogen evolution, and additive reduction.

In general, the control of an electrodeposition solution involves monitoring the concentration of additives and by-products of the reaction of additives at the electrodes.

1.5 ELECTROLESS AND DISPLACEMENT DEPOSITION

Electroless and displacement depositions have one basic characteristic in common: No power supply is necessary to drive the deposition reaction

$$M^{z+}_{solution} + ze \xrightarrow{\text{electrode}} M_{lattice} \tag{1.40}$$

In the electroless deposition process z electrons are supplied by a reducing agent, Red, present in the solution. The electron-donating species Red donates electrons to the catalytic surface. In the displacement deposition process z electrons are supplied by the substrate; the substrate S is the electron-donating species.

In general, an electrode with lower electrode potential in Table 1.1 will reduce ions of an electrode with higher electrode potential (Fig. 1.19).

1.5.1 Electroless Deposition

The overall reaction of electroless metal deposition is

$$M^{z+}_{solution} + Red_{solution} \xrightarrow{\text{catalytic surface}} M_{lattic} + OX_{solution} \tag{1.41}$$

where Ox is the oxidation product of the reducing agent Red. The catalytic surface may be the substrate S itself or catalytic

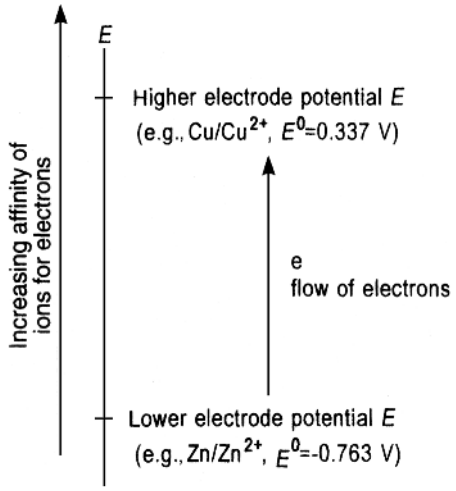

FIGURE 1.19 An electrode with lower electrode potential will reduce ions of an electrode with higher electrode potential.

nuclei of the metal M dispersed on a noncatalytic substrate surface. The reaction represented by Eq. (1.41) must be conducted in a way such that a homogeneous reaction between M^{z+} and Red, in the bulk of the solution, is suppressed.

According to the mixed-potential theory of electroless deposition [27–29] the overall reaction given by Eq. (1.41) can be decomposed into one reduction reaction, *the cathodic partial reaction*

$$M^{z+}_{solution} + ze \xrightarrow{\text{catalytic surface}} M_{lattice} \qquad (1.42)$$

and one oxidation reaction, *the anodic partial reaction*

$$Red_{solution} \xrightarrow{\text{catalytic surface}} Ox_{solution} + me \qquad (1.43)$$

Thus the overall reaction, [Eq. (1.41)] is the result of the combination of two different partial reactions, Eqs. (1.42) and (1.43). These two partial reactions, however, occur at one and the same electrode, the same metal–solution interphase. In order that the overall electroless deposition reaction may proceed, the equilibrium (rest) potential of the reducing agent, $E_{eq,Red}$ [Eq. (1.43)], must be more negative than that of the metal electrode, $E_{eq,M}$ [Eq. (1.42)], so that the reducing agent Red can function as an electron donor and M^{2+} as an electron acceptor. This is in accord with the discussion in Section 1.5.1.

Evans Diagram According to the mixed-potential theory, the overall reaction of the electroless deposition can be described electrochemically in terms of two current–potential *(i–E)* curves, as shown schematically in Figure 1.20. This figure shows a general Evans diagram with current–potential functions $i = f(E)$ for the individual electrode processes [Eqs. (1.42) and (1.43)]. In this the sign of the current density is supressed. According to this presentation of the mixed-potential theory, the current–potential curves for the individual processes $i_{cathodic} = i_M = f(E)$ and $i_{anodic} = i_{Red} = f(E)$ intersect. The coordinates of this intersection have the following meaning: (1) the abscisa, the current density of the intersection, is the deposition current density i_{dep} (i.e., log i_{dep}), that is, the rate of electroless deposition in terms of milliamperes per centimeter squared, and (2) the ordinate, the potential of the intersection, is the mixed potential, E_{mp}.

Mixed Potential, E_{mp} When a catalytic surface S is introduced into an aqueous solution containing M^{z+} ions and a reducing agent, the partial reaction of reduction [Eq. (1.42)] and the partial reaction of oxidation [Eq. (1.43)] occur simultaneously. Each of these partial reactions strives to establish its own equilibrium potential, E_{eq}. The result of this "competition" is the creation of a steady state with the compromised potential called the *steady-state mixed potential,* E_{mp}. The result of this mixed potential is that the potential of the redox couple Red/Ox [Eq. (1.43)] is raised anodically from the reversible value $E_{eq,Red}$ (Fig. 1.20), and the potential of the metal electrode M/M^{z+} Eq. (1.42) is depressed cathodically from its reversible value $E_{eq,M}$. down to the mixed potential E_{mp} (Fig. 1.20).

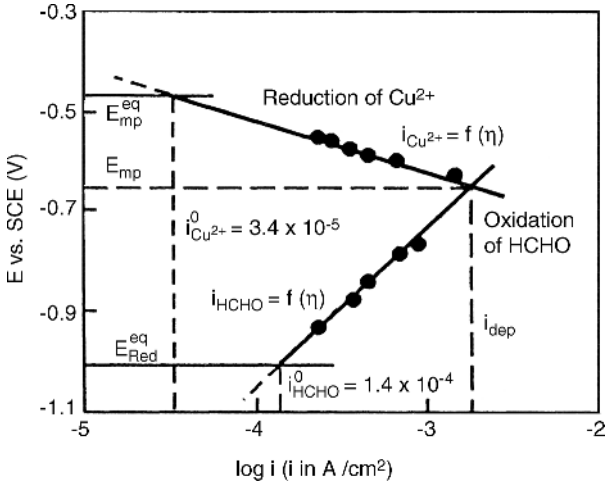

FIGURE 1.20 Current–potential curves for reduction of Cu^{2+} ions and for oxidation of reducing agent Red, formaldehyde, combined into one graph (Evans diagram). Solution for the Tafel line for the reduction of Cu^{2+} ions: 0.1 *M* $CuSO_4$, 0.175 *M* ethylenediaminetetraacetic acid (EDTA), pH 12.50, E_{eq}, $(Cu/Cu^{2+}) =$ 0.47 V versus saturated calomel electrode (SCE); for the oxidation of formaldehyde: 0.05 *M* HCHO and 0.075 *M* EDTA, pH 12.50, E_{eq} (HCHO) = 1.0 V versus SCE; temperature 25°C (±0.5°C). (From M. Paunovic, *Plating,* **55**, 1161 (1968), with permission from American Electroplaters and Metal Finishers Society.)

Mixed-potential theory was tested experimentally and verified extensivelly for the case of electroless deposition of Cu, Au, and Ni [1]. Its significance is in the fact that the kinetics and mechanism of clectroless deposition can be studied and interpreted by examining partial electrode processes [29].

1.5.2 Displacement Deposition

Section 1.5.1 mentioned that in the displacement deposition process z electrons in the deposition reaction [Eq. (1.40)], are supplied by the substrate. The substrate is the electron-donating species. We describe here an example of the displacement deposition of Cu on Zn which occurs when a strip of Zn is placed in a solution of $CuSO_4$. In order to find out what reactions will occur in this system, is necessary to consider standard electrode potentials (Table 1.1). The standard electrode potential E^0 of Cu/Cu^{2+} is 0.337 V and that for Zn/Zn^{2+} is -0.763 V. Since Zn/Zn^{2+} has a lower electrode potential than the Cu/Cu^{2+} system, Zn will reduce Cu^{2+} ions in the solution. Thus there are two partial reactions in this system, as in an electroless deposition system (Fig. 1.21). In displacement deposition of Cu on Zn, electrons are supplied in the oxidation reaction of Zn,

$$Zn \rightarrow Zn^{2+} + 2e \tag{1.44}$$

where Zn from the substrate dissolves into the solution and thus supplies electrons necessary for the reduction–deposition reaction

$$Cu^{2+} + 2e \rightarrow Cu \tag{1.45}$$

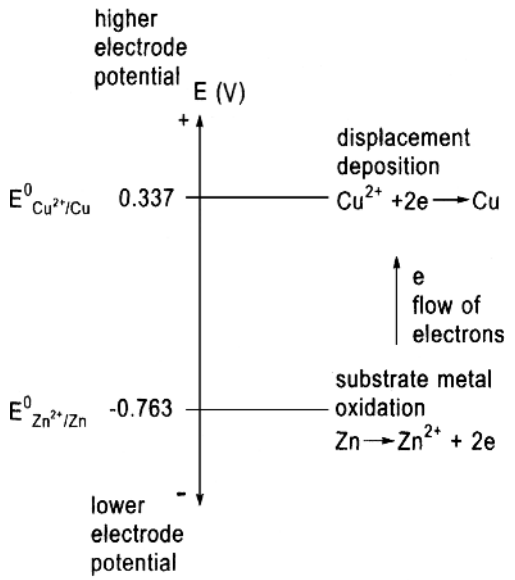

FIGURE 1.21 Relationship between partial reactions in displacement deposition of Cu on Zn, $Zn + Cu^{2+} = Zn^{2+} + Cu$.

The overall displacement deposition reaction is

$$Zn + Cu^{2+} \rightarrow Zn^{2+} + Cu \tag{1.46}$$

It is obtained by combination of the two partial reactions, oxidation and reduction, (1.44) and (1.45), respectively.

In general, Ox/Red (M^{z+}/M) couples with high standard electrode potentials are reduced by Ox/Red (M^{z+}/M) couples with low standard electrode potentials. In other words, low-potential couples reduce high-potential couples (see Table 1.1 and Fig. 1.19). The thickness of the deposited metal in this case is self-limiting since the displacement deposition process needs an exposed (free) substrate surface in order to proceed.

1.6 ELECTROLESS DIFFUSION BARRIER

Copper has been replacing Al in the fabrication of interconnects in chips due to the low-bulk electrical resistivity and superior electromigration resistance. The electrical resistance of pure Al and Cu are 2.9 and 1.7 mΩ-cm, respectively. Activation energies for electromigration are 0.81 ($\pm$ 0.03) and 1.1 ($\pm$ 0.03) for Al and Cu, respectively.

Copper introduces new problems, however, in the fabrication of interconnects on chips, the most important of which is possible diffusion of Cu into Si, Si dioxide, and the reaction of Cu with Si-forming silicides.

Thus, diffusion barrier layers are an integral part of the fabrication of Cu interconnects. Barrier layers can be represented schematically as

Si, Si dioxide–barrier layer–Cu

Yoshino et al. [29a] proposed an electroless NiB layer as the diffusion barrier layer.

In this process the reaction of electroless NiB deposition is activated by a self-assembled monolayer (SAM) containing Pd. Yoshino et al. found that this novel fabrication process yields high-quality film with high adhesion and satisfactory Cu barrier properties on low-k substrate. A low-k material is one with a small dielectric constant relative to silicon dioxide. In physics the symbol used for the dielectric constant is the Greek letter κ (kappa) while in semiconductor manufacturing the later-k is used.

It has been demonstrated that an electroless NiB film is effective as a barrier layer at a thickness as small as 20 nm.

1.7 PEG AND PPG AS SUPPRESSORS IN COPPER ELECTRODEPOSITION

The copper electrodeposition bath is typically a solution of cupric sulfate and sulfuric acid, containing a small concen-

tration of chloride ions. As explained in Section 1.6 the electrodeposition of copper is currently the method of choice for on-chip production of interconnects in microelectronics. Copper is electrodeposited in submicrometer trenches and vias. In order to get copper of high quality, a deposition suppressor is used.

Polyethylene glycol (PEG) and polypropylene glycol (PPG) or a combination of the two is used as suppressor. The original paper [29b] treats PEG, PPG, and their triblock copolymers, but here we are limited to PEG and PPG. The suppressor increases the overpotential for copper ion reduction by a surface adsorption interaction with chloride ions. Polypropylene glycal is causing great suppression in the copper deposition current, but using a mixture of PEG and PPG indicates that PEG dominates when both suppressors are present. Competitive adsorption is capable of explaining the mechanism of suppression.

In the absence of adsorption reduction the reaction of Cu ions is given by

$$i = i(0)\exp\left(\frac{-\eta}{b}\right) \tag{1.47}$$

where i (0) is the exchange current density, η is the electrode overpotential, and b is the Tafel slope (Section 1.3.1).

When competitive adsorption is present, the reduction current for Cu is given by

$$i(\text{ads}) = i(0)[1-\theta(\text{eff})]\exp\left(\frac{-\eta}{b}\right) \tag{1.48}$$

where θ(eff) is the effective surface coverage. Dividing Eq. (1.48) by Eq. (1.47) results in

$$\theta(\text{SS}) = 1-\left(\frac{i(\text{ads})}{i}\right) \tag{1.49}$$

where θ(SS) is the effective steady-state coverage. The available surface sites are given by $1 - \theta$(SS).

1.8 INFLUENCE OF ADDITIVES AND THE EFFECT OF AGING IN ELECTRODEPOSITED COPPER

In Section 1.4.1 we described the effect of additives on the deposition and crystal-building process as adsorbates (adsorbed substances) at the surface of the cathode.

In this section we describe the influence of additives and the effect of aging in modifying surface topography of electrodeposited copper [29c]. As a result of room temperature aging there is a change in the grain size and the microstructure of the copper deposit.

The X-ray diffraction patterns of the copper deposit exhibits a prominent (111) orientation in addition to (200), (220), and (311) planes. However, during room temperature aging copper deposit has a prominent (200) plane orientation.

The authors used scanning electron microscopy (SEM) and atomic force microscopy (AFM) in order to follow the influence of additives and the effect of aging.

On analysis SEM showed that the deposits have round or globular features and there is a change in grain size related to a particular additive. Additives used are PEG (Section 1.7), chloride ion, and PEG and chloride ion.

Atomic force microscopy showed that the average grain size strongly depends on the deposition rate and the type of additive. Additives used are the same as studied with SEM. It was found that there is a change in the grain size and the morphology of the copper deposit due to the room temperature aging.

PART B PHYSICAL CONSIDERATIONS

1.9 ELECTRODEPOSITION OF ALLOYS

1.9.1 General

Alloy deposition is as old an art and science as the electrodeposition of individual metals (e.g., brass, which is an alloy of copper and zinc, deposition was invented circa 1840). As can be expected, alloy deposition is subject to the same principles as single-metal plating. Indeed progress in both types of plating has depended on similar advances in electrodeposition science and/or technology. The subject of alloy electroplating is being dealt with by an ever-increasing number of scientific and technical publications. The reason for this is the vastness of the number of possible alloy combinations and the concomitant possible practical applications.

Properties of alloy deposits superior to those of single-metal electroplates are commonplace and are widely described in the literature. In other words, it is recognized that alloy deposition often provides deposits with properties not obtained by employing electrodeposition of single metals. It is further the case that, relative to the single-component metals involved, alloy deposits can have different properties in certain composition ranges. They can be denser, harder, more corrosion resistant, more protective of the underlying basis metal, tougher and stronger, more wear resistant, different (better) in magnetic properties, more suitable for subsequent electroplate overlays and conversion chemical treatments, and superior in antifriction applications.

Electrodeposited binary alloys may or may not be the same in phase structure as those formed metallurgically. By way of illustration, we note that in the case of brass (Cu–Zn alloy), X-ray examination reveals that, apart from the superstructure of β-brass, virtually the same phases occur in the alloys deposited electrolyticalty as those formed in the melt. Phase limits of electrodeposited alloys closely agree with those in the bulk form. Somewhat opposite is the case of the Ag–Pb alloy. In the cast alloy form it contains "large" silver crystals with lead present in the grain boundaries as dendrites. In the electrodeposited form the alloy contains exceedingly fine grains exhibiting no segregation of lead.

By choosing specific metal combinations, electrodeposited alloys can be made to exhibit hardening as a result of heat treatment subsequent to deposition. Such treatment, it should be noted, causes solid precipitation. When alloys (e.g., Cu–Ag, Cu–Pb, and Cu–Ni) are coelectrodeposited within the limits of diffusion currents, equilibrium solutions or supersaturated solid solutions are in evidence, as is observed by X-ray analysis. The actual type of deposit can, for instance, be determined by the work value of nucleus formation under the overpotential conditions of the more electronegative metal. When the metals are codeposited at low polarization values, the formation of solid solutions or of supersaturated solid solutions results. This is so even when the metals are not mutually soluble in the solid state according to the corresponding phase diagram. As a rule, codeposition at high polarization values, on the other hand, results in two phase alloys even with systems capable of forming continuous series of solid solutions.

1.9.2 Principles

The electrodeposition of an alloy requires, by definition, the codeposition of two or more metals. In other words, their ions must be present in an electrolyte that provides a "cathode film" where the individual deposition potentials can be made to be close or even the same,

Three main stages in the cathodic deposition of alloys (or single metals) are to be recognized:

1. *Ionic Migration* The hydrated ion(s) in the electrolyte migrate(s) toward the cathode under the influence of the applied potential as well as through diffusion and/or convection.
2. *Electron Transfer* At the cathode surface area, the hydrated metal ion(s) enter the diffusion double layer where the water molecules of the hydrated ion are aligned by the field present in this layer. Subsequently the metal ion(s) enter(s) the fixed double layer where, because of the higher field present, the hydrated shell is lost. Then on the cathode surface the individual ion may be neutralized and is adsorbed.
3. *Incorporation* The adsorbed atom wanders to a growth point on the cathode and is incorporated in the growing lattice.

1.9.3 Deposition

Now the deposition potential, which is the potential at which deposition occurs for a given metal, is determined by two major quantities, as was discussed in the first part of this chapter [see Eqs. (1.3) and (1.4)]. Specifically, one quantity is the standard electrode potential, E° (it is defined as the potential that exists when the metal is immersed in a solution of its ions at unit activity) which is a characteristic of the metal in question. The other quantity is a function of the ion's activity value in the electrolyte. This value is in turn proportional to the ionic concentration as long as the latter is of moderate value; otherwise, it is a complicated function of all the units in the solution. For two metals to be codeposited and thus produce an alloy, they must both be present in the electrolyte, and their individual deposition potential should be the same or nearly the same. It is clear that for two metals whose standard electrode potentials differ by a great amount, the only way to achieve these deposition potentials is by controlling the value of the activity, that is, changing the respective concentrations. The deposition potentials can thus be brought into harmony. Detailed calculations (see *Fundamentals*), for instance, indicate that copper ion concentration can be brought into harmony with zinc ion concentration in certain solutions and thus can be used in Zn–Cu alloy plating.

Using an example, we wish to stress the point that in a solution containing "simple" salts of zinc and copper where ion concentration, and so the activity, values are close together, an alloy deposition is virtually impossible. That is due to the large difference between the standard electrode potentials E^0 for copper (-0.345 at 25°C) and that for zinc (-0.762 at 25°C).

In a mixed copper–zinc solution of complex cyanide, however, the Cu^+ ion concentration can be reduced to the order of 10^{-18} mol L^{-1} and the concentration ratio (zinc ion)/(copper ion) will be made very large. This will compensate for the large difference in their standard electrode potentials. A detailed treatment for this case shows that copper cyanide complex is of the form $Cu(CN)_4^{2-}$ for which the dissociation constant value is known. The dissociation constant for the zinc cyanide complex $Zn(CN)_4^{2-}$ is also well known. Calculations using these values make it clear that their respective deposition electrode potentials can be brought close enough together.

To express the above in a different, more specific way, we state that codeposition of two or more metals is possible under suitable conditions of potential and polarization. The necessary condition for the simultaneous deposition of two or more metals is that the cathode potential–current density curves (polarization curves) be similar and close together.

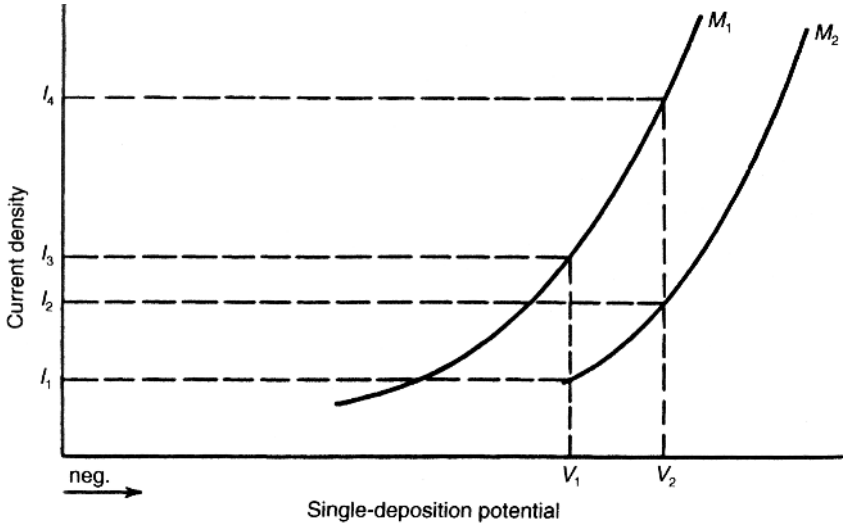

FIGURE 1.22 Single-electrode potentials of metals M_1, and M_2 versus current density in the same type of bath.

Figure 1.22 depicts a typical deposition potential plotted against current density for two different individual metals. The curves indicate that in a bath containing both metals, M_1 and M_2, may codeposit at, say, potential V_2 in the ratio I_4/I_2.

It should be understood that the plating bath may be depleted of one metal ion faster than of another. In order to keep deposition conditions under control, (uniform), metal ions must be replenished in direct proportion to their rates of deposition dictated by the specific alloy. Clearly, the ideal case is where the polarization curves of the component metals being codeposited are identical. In practice, however, it is next to impossible to realize this condition.

Electrochemically viewed, even when a single-metal deposition is accompanied by hydrogen evolution, it may well be said that one deals with alloy plating in which hydrogen is the codepositing element. This is equally so when hydrogen is discharged as gas, since the conditions for codeposition are met. Alloy plating of metals makes it into a process of production of hydrogen and the two or more metals that are being alloyed.

Another path to alloy deposition is that via interdiffusion in electrodeposited bilayers or multilayers. In this case different coatings are deposited alternately using two different plating baths or even one bath where the deposition potential is varied periodically and then heat treatment is applied to promote mutual diffusion, thus ending up with an alloy. For example, an alloy of 80% Ni and 20% Cr can be produced by the deposition of alternating layers of 19-μm-thick Ni and 6-μm-thick Cr. Subsequent heating to 1000°C for 4–5 h produces completely diffused alloys of rather high quality in terms of their corrosion properties. Brass can also be produced by interdiffusion of Cu and Zn under suitable conditions.

1.10 STRUCTURE AND PROPERTIES OF DEPOSITS

1.10.1 General

In their solid state, atoms (ions) are arranged in a regular pattern that may be described by the three-dimensional repetition of a certain pattern unit. The structure therefore is said to be periodic. When the periodicity of the pattern extends throughout a piece of the material, we refer to it as a *single crystal.* In polycrystalline material the periodicity is interrupted at so-called grain boundaries. The size of grains through which the structure is periodic varies markedly, as discussed below. When the size of the grains or crystallites becomes comparable to the size of the pattern unit, the substance is called *amorphous.*

Grains are understood here to be individual crystallites in a polycrystalline body of material. This definition, however, is not common to all authors. Thus some authors refer to clumps of crystallites as "grains" while others call such clumps "islands."

Crystalline material, as stated above (whether single-crystal, polycrystalline, or even nanocrystalline amorphous), is made such that its component (constituent-based) ions. atoms, or molecules are arranged on a three-dimensional regular, repetitive pattern called a *lattice.* In metals the constituent bases are singly or multiply ionized metal atoms. The commonest form among (plated) metals is the face-centered-cubic (fcc) lattice, which is the lattice structure of Ag, Al, Au, Cu, Ni, and others. Here fcc refers to a lattice arrangement of metal ions at each of the corners of a cube plus one atom each in the center of every cube face.

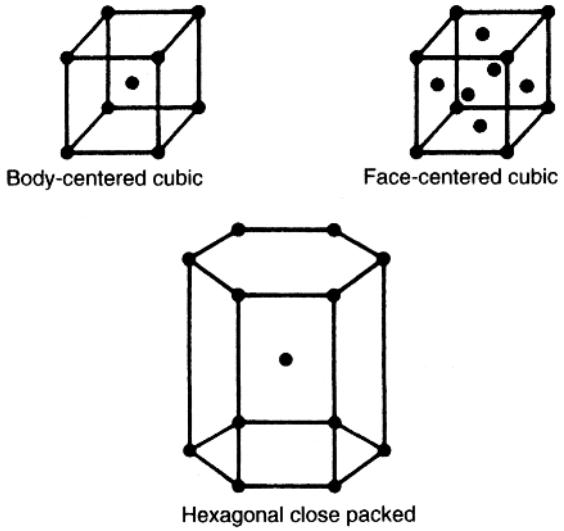

FIGURE 1.23 Unit cells of the three most important lattices. (From C. Kittel, *Introduction to Solid State Physics*, 6th ed., Wiley, 1986. Reproduced with permission.)

Next in frequency is the hexagonal close-packed (hcp) lattice, which is assumed by Co, Zn, and some others. Here hcp refers to an arrangement of metal ions with planes of ions placed at the corners of hexagons which are separated by planes of ions grouped in sets of three between hexagons in the adjacent planes. This way one of the two close-packing arrangements of hard spheres is realized. The other way of close packing of hard spheres is realized by the fee arrangement. That arrangement is therefore sometimes referred to as *cubic close packed.*

The body-centered-cubic (bcc) is the lattice symmetry of Fe, for instance. Here bcc refers to a crystal arrangement of ions at the corners of a cube and one ion in the center of the cube equidistant from each face. Figure 1.23 depicts the unit cells corresponding to the above-mentioned structures. In the last analysis, the crystalline structure exhibited as a product of electrodeposition depends on a "competition" between rates of new crystallite formation and existing crystal growth.

It ought to be stressed that actually a large number of variables in the plating process have bearing on structure. Among these are metal ion concentration, additives, current density, temperature, agitation, and polarization. It is outside the scope of this chapter to discuss these effects in more detail.

1.10.2 Substrate and Environment

Another factor that has substantial influence on electrodeposits, their structure, and their properties is the nature of the substrate upon which the plating occurs. Two phenomena are important in this context: *epitaxy* and *pseudomorphism.* Epitaxy refers to the systematic structural kinship between the atomic lattices of the substrate and the deposit at or near the interface. In other words, it concerns the induced continuation of the morphology and/or structure of the substrate material into a coating applied on to it. An important parameter of epitaxial growth is the substrate's temperature. For a given material being deposited on a substrate, all other conditions being fixed, there exists an *epitaxial temperature.* That is a temperature above which epitaxial growth is possible; below this temperature no epitaxial growth can occur. For example, for silver evaporated on NaCl, the temperature is 150°C, Pseudomorphism is the continuation of grain boundaries and similar geometric features of the substrate into the deposit. An alternative definition states that deposits that are stressed to fit upon a substrate are said to be pseudomorphic. A working rule is that pseudomorphism persists deeper (up to 10 nm) into the deposit than epitaxy.

Prior cleaning, or the cleanliness state of the substrate, also greatly influences the structure and adhesion of the deposit. In general, both mechanical and chemical cleaning methods may be required.

Metal surfaces exposed to certain types of gas will generally undergo transformation, and their transformation can be accompanied by significant changes in their properties. The rate and the extent of change are dependent on the metal, the gases, and the new phase/product that will form at the interface between the two original phases. We mention here the case of Si oxidizing to form SiO_2 which undergoes expansion, thus creating strong (compressive) stress on the interfacial surface.

An example of high practical significance is the copper deposits used in microelectronics, mirrors, and other optical applications. These deposits have been observed to soften over time even when stored at room temperature for as short as four to six weeks. The surfaces of mirrors and other precision objects made of copper will deform after a few months. This kind of degradation can be counterweighed by a suitable metal overcoating. Another, though not always practical, way is to subject the object to heat treatment at about 300°C. These degradation phenomena are the direct results of microstructural instabilities, often referred to as *recrystallization* in the copper. It is worth stressing that recrystallization is not limited to copper. "As-deposited" electroless Ni–P is subject to a similar process.

Crystals grown via electroplating may be oriented every which way. That is to say, the direction axes of individual crystallites may be randomly distributed. The case, however, where one axis is oriented or fixed in *nearly* one direction is said to be a single texture. Where two axes are fixed or oriented, it is said to be double texture. Monocrystalline orientation refers to the case where there are three such nearly oriented axes. This includes, for instance, epitaxial films. Orientation is viewed with respect to any fixed (in space) frame of reference.

Electrochemical parameters, and not substrate properties, are the main deciding factors in the texture of deposits. This is particularly evident if the deposit's thickness is 1 μm or more. In deposits of lesser thickness, the substrate plays an important role as well (see above). Another nonelectrochemical factor may be the codeposition of particulate matter with some metal deposits. To summarize, we note that texture is mostly influenced by deposition current density, itself being a function of bath parameters. Not surprising, then, is the fact that in the case of physical vapor deposition (PVD) the deposition rate, which serves as the effective current density, is the determining factor in setting the texture of the coating.

1.10.3 Properties

The functional relationship between structure and property is complex. To be precise, there are different microscopic and macroscopic interactions involved in materials. There are both quantum-mechanical interactions between constituent atoms or molecules and classical-type interactions between grains and groups of grains. Electrodeposition adds some measure of complication since it is inherently a nonequilibrium process. The product films thus exhibit many imperfections that vary in number and nature from grain to grain. In this connection it is also important to remember that the most basic imperfection of a crystal lattice is the surface itself where the periodicity, the hallmark of bulk material, is cut off.

For illustration of the complexity discussed above, we note the following few practical cases:

1. Gold, when electrodeposited with about 0.5% cobalt, has a hardness of about four to five times that of annealed electrodeposited gold. This degree of hardness cannot be achieved using any of the known metallurgical methods. It is widely believed that grain sizes of 20–30 nm in this material are responsible for this high degree of hardness. Cobalt-hardened gold films have found a large number of applications in electronics and other areas.
2. Texture has a marked influence on the properties of a given deposit. Seemingly unrelated parameters (properties) such as corrosion resistance, hardness, magnetic properties, porosity, and contact resistance are all texture dependent. The specific texture of a copper substrate upon which a nanomultilayer system such as Cu–Ni layer pairs are deposited has direct bearing on the deposit's texture and consequently magnetic characteristics.
3. Different nickel deposits show a great variety of contact resistance values. This is particularly so after the deposits have been exposed to the atmosphere for extended periods of time. The differences in these values may be best explained in terms of variations in plated texture. Nickel electrodeposits with polycrystalline nature have been observed to behave as single crystals if their grains are oriented such that the (100) planes are parallel to the surface. Not surprisingly the oxidation rate in (100) oriented single crystals is self-limiting at ambient temperature.
4. The optical properties of some thin-film light polarizers owe their ability to polarize light to the specific texture of their structure.

1.10.4 Impurities

Electroplated films almost always contain various types of inclusions or impurities. These additives may be from one or more of the following origins:

1. Added chemicals (levelers, brighteners, etc.)
2. Added particles (for composite coating)
3. Cathodic products (complex metal ions)
4. Hydroxides (of the depositing metals)
5. Bubbles (e.g., hydrogen gas)

In general, it may be stated that deposits produced using low current densities possess higher impurity content than deposits produced using high current densities (see *Fundamentals*).

Small amounts (in ppm) of impurities can also influence material strength. For example, as noted earlier, a small amount of cobalt in electrodeposited gold enhances its hardness. Sulfur impurities can, on the other hand, be detrimental to nickel deposits. An increase in sulfur content is known to reduce the fracture resistance of electroformed nickel. If no other impurities are present in the electrodeposited nickel, hardness alone can be used as an indicator of sulfur impurity content.

From the foregoing discussion it should be clear that in practice it is virtually impossible to obtain and maintain electrodepositing baths free from impurities. This is a big consideration in the research laboratory. In research work on electrode kinetics, for example, careful and often complex purification procedures are followed in order to remove some key contaminants. Otherwise, no reproducible or reliable results can be obtained. The plating shop worker, on the other hand, deals with highly contaminated (from the point of view of the researcher) solutions from a variety and by and large unknown sources. It is for this reason that technical practice must and does rely on empirical observations.

In some deposits, notably those of nickel, electrical resistance follows current density at low temperatures in the sense that films deposited at a low current density (e.g., 10 mA cm^{-2}) show lower resistance than those deposited at higher density.

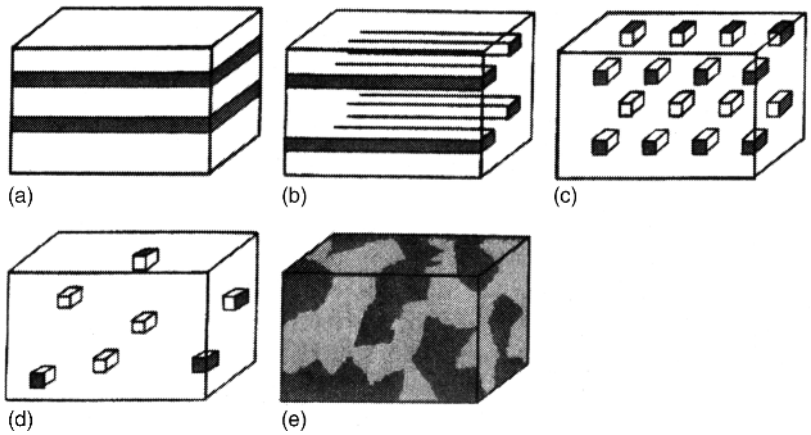

FIGURE 1.24 (a) Quantum wells, multilayers; (b) quantum wires; (c) ordered dots; (d) random dots; (e) nanometer-sized dots.

This effect of low resistance occurs in the low-temperature range of 4–40 K but disappears at closer to room temperature.

A special type of impurity is hydrogen. Hydrogen is codeposited with most metals. Because of its low atomic number, it can be expected to be readily adsorbed by the basis metal. The source of the hydrogen may vary from the associated preparatory processes such as electrocleaning to the specific chemical reactions associated with the plating process itself. Regardless of its origin the presence of hydrogen may result in embrittlement, which means a substantial reduction in ductility. Hydrogen embrittlement (HE) is an expression used to describe a large variety of fracture phenomena having in common the presence of hydrogen in the metal or alloy as a solute.

Many types of mechanisms have been suggested in the attempts to explain HE in different systems. No consensus has been reached to date as to the validity of these. The absorbed hydrogen in steel, for instance, makes it most susceptible to embrittlement. At least in part, this is due to the hydrogen interfering with the normal flow or slip of the lattice planes under stress. If, as often is the case, a deposit contains voids on the microscopic scale, hydrogen may accumulate in molecular form possibly developing pressures exceeding the tensile strength of the basis metal leading to the development of blisters.

Finally, in physical vapor-deposited as well as sputter-deposited films, incorporated gases can increase stress and raise annealing temperatures. Similar effects are present in electron-beam-evaporated films.

1.11 MULTILAYERED AND COMPOSITE FILMS

1.11.1 General

With the introduction of many different reliable ways, including electrodeposition, to produce systems with nanometer- scale structural and composition variations, there has come the ability for greater control of material properties, which has led to the design of new materials.

Nanostructural materials are divided into three main types: one-dimensional (commonly known as multilayered) structures made of alternate thin layers of different composition; two-dimensional structures (commonly known as wire-type elements suspended within a three-dimensional matrix); and three-dimensional constructs which may be made of a distribution of fine particles suspended within a matrix (either in periodic or random fashion) or an aggregate of two or more phases with a nanometer grain size. Figure 1.24 depicts the above-mentioned constructs.

The semiconductor community has made band gap engineering a reality by exploiting the ability to produce multiple quantum well material. Here the quantum well refers to a potential well with dimensions such that quantum-mechanical effects are taken into account. In other words, one thinks of electrons/holes as being trapped in the well, having distinct energy levels rather than a continuum. The progress from one-dimensional nanostructural materials to two- and three-dimensional ones (i.e., to quantum wires and quantum dots; see Fig. 1.24) has provided enhanced carrier (electrons and/or holes) confinement by their presence, which permits more control of the energy band structure.

Accurate control of a microstructure on the nanometer scale makes it possible to control magnetic and mechanical properties to a hitherto unattainable degree. In particular, magnetic nanostructures have recently become the subject of an increasing number of experimental and theoretical studies. The materials are made of alternating layers, around 10 Å thick, of magnetic (e.g., cobalt) and nonmagnetic metals (e.g., copper).

The magnetic layers are exchange coupled to one another with a sign that oscillates with the thickness of the spacer (nonmagnetic) layer. This arrangement can be understood if one considers the multilayer systems as magnetic layers separated by nonmagnetic layers. The number of free conduction electrons is dependent on the number of nonmagnetic

atoms, that is, the thickness of the nonmagnetic layer. As this number increases, subsequent orbitals in the magnetic atoms will experience alternating electron surpluses and deficits, causing a sinusoidal variation in the average magneton number per atom. Thus the magnitude of the exchange interaction varies not only in the usual fashion, inversely with the square of the distance between magnetic layers, but also in a sinusoidal manner. These results were known recently for sputtered, evaporated, and molecular beam epitaxy (MBE) grown samples.

Electrodeposition of composition-modulated films was first performed by Brenner in 1939 [30], who employed two separate baths for the two components and a "periodic" immersion of the deposit in the two baths. This method proved too cumbersome to be adopted in practice, however. Deposition from a single bath with the presence of salts of the two components of the multilayer is what has evolved.

A serious problem was found in the deposition of two metals from one bath. Specifically, while a layer of the more noble member could be deposited by choosing the potential to be between the reduction potentials of the two metals, the potential had to be set to a value appropriate for the reduction of the less noble member so that both would be deposited and result in an alloy layer rather than a pure metal.

1.11.2 Electrodeposition of Nanostructures

In 1986 Yahalom and Zadok [31] pointed to methods to produce composition-modulated alloys by electrodeposition, initially for the Cu–Ni couple. Modulation was obtained to thicknesses down to 8 Å. The principle of their method follows.

Traces of metal A ions are introduced into a concentrated solution of metal B, assuming that metal A is nobler than B. At a low enough polarization potential the rate of reduction of metal B is high because it is determined by its activation polarization. The rate of reduction of metal A is slow and controlled by diffusion. At a predetermined considerably less negative polarization potential only metal A is reduced. The potential is simply switched between these two potential values, forming a modulated structure composed of pure A layers and layers of B with traces of A in the B layers. The actual deposition of the multilayered composite can be carried out by either current or potential control.

The method is suitable for a considerable number of metal couples. The main caveat, however, is that both metals can be deposited from similar baths. Another is that they differ sufficiently in their degree of nobility.

The method was first tried using the Cu–Ni system, which is still the most-studied system by far when it comes to electrochemically produced layered structures. The reasons for this are quite compelling. There is a sufficient difference in reduction potentials of the two metals. There is the similarity in crystal structure (fcc) and proximity of lattice parameters, ensuring a good coherency between the layers. Further considerable data exist on the magnetic, mechanical, and other properties of the Cu–Ni system deposited by other than electrodeposition, enabling comparison of the modulated layers produced by the chemical method.

1.11.3 Analysis of the Deposit

A standard method for confirming the coherence of the layers is via X-ray diffraction spectra. If the layers are coherent and there are a sufficient number of them to provide a relatively strong Bragg diffraction pattern, then satellites due to superlattice formation should appear on each side of the Bragg diffraction peak (superlattice refers here to the periodicity of the layered structure).

The mathematical expression for the difference between the sine values of the two satellites is

$$\sin\theta_s^+ - \sin\theta_s^- = \frac{\lambda}{\Lambda}$$

where λ is the X-ray wavelength and Λ is the superlattice repetitive period. The expression is a consequence of an analogous formula for light diffraction by optical grating.

In general, one can expect systems like these to have properties different from the bulk. In bulk materials, most ions are in a crystalline environment; that is, they do not "see" the surface. In a crystalline superlattice most atoms "know" they are near an interface, that is, in a noncrystalline/nonperiodic environment. For an extended treatment of the mechanical, magnetic, and other properties of muitilayered thin-film systems, the reader should consult *Fundamentals* (Chapter 17).

1.11.4 Conclusion

All the possible methods of deposition have inherent advantages and disadvantages with regard to the quality of the multilayers they create and the ease of their production. However, electrodeposition seems best to fulfill imposed financial and temporal restrictions. Specifically, vapor deposition is expensive, creates quasiamorphous interfaces, and is time consuming in terms of controlling the alternation of deposition material. Electroless deposition may suffer from the same drawback with regard to mechanical switching between solutions for alternating layer materials. Finally, sputtering requires an expensive vacuum system and cannot easily be extended to industrial usage. For these reasons electrodeposition is now the production method of choice for most practical needs.

The constructs thus obtained provide a useful paradigm for fundamental studies as well as for a plethora of applica-

tions. Some applications are in magnetically operated read/write heads, others in sensors, but these are just a precious few. Recently (January 1998) IBM became the first company to market giant magnetoresistance (GMR)–based multilayer read/write heads in a family of disc drive products designated Deskstar 16 GP. The use of such technology allows the reading and writing of extremely small magnetic bits of information that facilitates high-density storage. This provides for the ability to store 3.2 gigabytes of data on a 95-mm-diameter disc.

We must again emphasize that electrodeposition presents, in principle, several advantages for the investigation and production of layered alloys. Among these characteristics are the tendency of electrodeposited materials to grow epitaxial and thus to form materials with a texture influenced by the substrate. Electrodeposition thus can be used in systems that do not lend themselves to vacuum deposition. The electrodeposition process is inexpensive, and it can be scaled up with relative ease for use on large parts; further it is a room temperature technology. This last point is important for systems in which undesirable interdiffusion between the adjacent layers may readily occur.

The studies so far of electrodeposited multilayer materials clearly show that electrodeposition is a viable technique for the production of thin muitilayered materials in systems that, from the electrochemical standpoint, are adaptable to the pulsed deposition technique.

Recent results have been able to demonstrate that the coatings produced by electrodeposition display the same coherency and layer thickness uniformity as those composition-modulated alloys produced by vacuum evaporation or sputter deposition. Demonstration of the capability of electrodeposition to produce materials with predesignable, variable, and controllable composition down to practically the atomic scale constitutes an important step toward the realization of custom-tailored materials. On the theoretical side, the lack, at the time of writing, of a single satisfactory theory for the possible explanation of the ever-growing amount of empirical results is still somewhat disappointing and surprising.

1.12 INTERDIFFUSION IN THIN FILMS

1.12.1 General

Modern integrated circuits are made of layered thin-film structures which are subject to interdiffusion during the thermal processing stage in fabrication. Diffusion, in general and not only in the case of thin films, is a thermodynamically irreversible self-driven process. It is best defined in simple terms such as the tendency of two different gases to mix when separated by a porous partition. It drives toward an equilibrium, maximum-entropy state of a system. It does so by eliminating concentration gradients of, for instance, impurity atoms or vacancies in a solid or between physically connected thin films. In case of two gases separated by a porous partition, it leads to the eventual perfect mixing of the two.

In equilibrium in a solid, the impurities or vacancies will be distributed uniformly. Similarly, in the case of two gases, as above, once a thorough mixture has been formed on both sides of the partition, the diffusion process is complete. As well at that stage, the entropy of the system has reached its maximum value by virtue of the fact that the *information* regarding the whereabouts of the two gases has been minimized. In general, it ought to be remembered that entropy of a system is a measure of the information available about the system. Thus the constant increase of entropy in the universe, it is argued, should lead eventually to an absolute chaotic state where no information is available at all.

The diffusion process in general may be viewed as the model for specific, well-defined transport problems. In particle diffusion, one is concerned with the transport of particles through systems of particles in a direction perpendicular to surfaces of constant concentration. In a viscous fluid flow, one is concerned with the transport of momentum by particles in a direction perpendicular to the flow. In electrical conductivity it is with the transport of charges by particles in a direction perpendicular to equal potential surfaces. In solids, for instance, the chemical potential is identified with the Fermi energy level. When two solids or thin films are brought into contact, such as in the case of a *p–n* junction, charged particles will undergo interdiffusion such that the chemical potentials or Fermi levels will be balanced, that is, reach the same level.

Let us assume now that particle diffusion occurs as a result of the difference in concentrations, as is the case in a deposition bath. Then a relation known as *Fick's law* is in effect, and it is written as

$$\text{Particle flux} = (\text{diffusion coefficient}) \times (\text{driving force})$$

or using the language of mathematics,

$$J_n = -D \operatorname{grad} c \tag{1.50}$$

where c is the concentration of the diffusing species (ions or particles). The concentration gradient is acting as the driving force.

The term *flux* here refers to the amount of the diffusing substance passing through a cross section of unit area in unit time. The term *gradient* refers to the change in substance concentration as a function of distance. Both quantities, since they have directionality in addition to a numeric value, are viewed as vector quantities. It has been found experimentally that the diffusion constant/coefficient, D in Eq. (1.50), depends on temperature according to an exponential-type

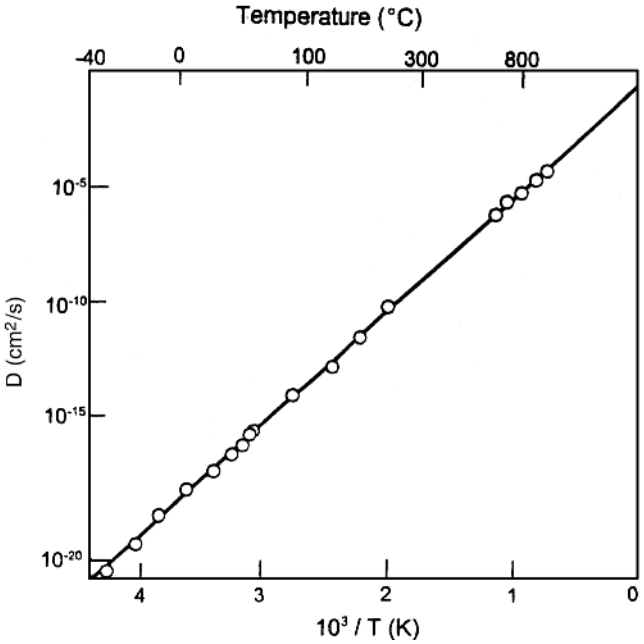

FIGURE 1.25 Diffusion coefficient of carbon in alpha iron. (From C. Kittel, *Introduction to Solid State Physics*, Vol. 7, Wiley, New York, with permission from John Wiley & Sons.)

expression (see Fig. 1.25), This type of temperature dependency is indeed typical of activation energy driven processes, in general.

To actually diffuse, an atom ion must overcome a potential energy barrier due to neighbors. If, as above, the potential energy barrier height is E, then the statistical mechanical considerations indicate that the atom will have sufficient thermal energy to pass over the barrier a fraction $\exp(-E/kT)$ of the time. Here T stands for the absolute (Kelvin) temperature while k is Boltzmann's constant. If f is a characteristic atomic vibrational frequency, then the probability p that during unit time the atom will pass the potential energy barrier is given by

$$p \cong f \exp\left(\frac{-E}{kT}\right) \tag{1.51}$$

In other words, in unit time the atom makes f (of the order of $10^{14}\,s^{-1}$) attempts to surmount the barrier with the probability each time of the exponent. Thus the quantity p is also known as *jump frequency*.

1.12.2 Diffusion in Electrodeposits

Diffusion is liable to corrupt the properties of a deposit and defeat the purpose for which the electrodeposition was performed in the first place. This may particularly be so at the basis metal–film interface. Thus, for instance, in deposits for decorative purposes, diffusion of the coated underlayer (metal) to the surface will debase the intended appearance. Another example is gold plating of electronic contacts, which is often practiced in order to avoid corrosion of the contact areas. In gold plating the underlayer is often copper. The copper can diffuse to the surface of the gold. As a result of the copper oxidation the contact resistance will be altered and markedly for the worse. As a practical fact we note here that a 3-μm-thick gold film deposit will be covered with the oxide of its underlying copper if exposed to 300°C within one month. If exposed to 500°C a gold layer of 30 μm thickness will be diffused through in four to five days.

In some instances, to improve solder ability, tin is deposited on nickel surfaces. In a short time, however, interdiffusion of the two metals results in the growth of an intermetallic $NiSn_3$ compound that is much less amenable to soldering. In the case of tin electrolessly deposited over nickel surfaces, the interdiffusion results in pores in both films. Pores are to be avoided, of course, if conductivity or contact resistance is an issue.

Earlier in this chapter mention was made of hydrogen embrittlement. It was indicated that the presence of hydrogen in, say, steel will result in the same effect. That predicament concerns an interstitial solid solution. The solute atoms (hydrogen in this case) may move along the interstices between the solvent atoms (iron in this case) without having to displace them. This state of affairs is facilitated by the hydrogen atoms being much smaller than the interionic space in the lattice of the solvent.

Diffusion must not, however, always be viewed as a harmful phenomenon. In some cases it is desirable, if not essential, as in welding, where diffusion ensures joining of the welded parts. Steel is often coated with tin to protect it from corrosion. In this case the formation, via interdiffusion, of the intermetallic $FeSn_2$ is the key for effective protection.

Yet another positive aspect of the diffusion phenomenon is the creation of alloys by first depositing alternate layers of different coatings, and then an alloy is created by heating to promote interdiffusion to produce an alloy. Specifically brass deposits can be produced by first depositing copper and zinc layers alternately. Subsequent heating produces the required brass. This type of approach obviates the undesired direct method of brass deposition via a cyanide process.

In the case of jet engine parts which are routinely subject to temperatures close to 500°C, diffusion-alloyed nickel–cadmium is found to serve as an effective corrosion protective agent.

1.12.3 Void Formation

Whenever the interdiffusion of two metals is uneven, it can create vacancies or voids. The uneven diffusion is the result of unequal mobilities between a metal couple. The voids

occur individually near the common interface. Voids like bubbles coalesce, resulting in porosity and loss of strength. Many thin-film couples exhibit this phenomenon, which is referred to as *Kirkendall void creation*. A few examples are Al–Au, Cu–Pt, and Cu–Au. To be specific, it has been found, for instance, that in Au–Ni about five times more Ni atoms diffuse into Au than Au atoms diffuse into Ni.

Kirkendall void formation can, however, be prevented from occurring by choosing the "right" metal species. For instance, while platinum coating upon copper is subject to the Kirkendall void creation process, the same coating upon electrodeposited nickel is free of it, even if the surface is heated to as high as 600°C for many hours (more than 10 h).

Again, the effect has useful aspects as well. It can help in controlling porosity, say, of an electroformed object requiring cooling. Indeed, this is a consideration in a number of electronics applications.

1.12.4 Diffusion Barriers

Diffusion barriers are coatings that serve to protect against undesirable diffusion. One of the best examples is that of a 100-μm-thick electrodeposited copper layer. That serves as an effective barrier against the diffusion of carbon. Another example is nickel and nickel alloys (notably electrolessly deposited Ni–P) that block diffusion of copper into and through gold over plate. This is achieved by the deposition of a relatively thin Ni–P layer (less than 1 μm) between the copper and its overlayer. Naturally the effectiveness of the diffusion barrier increases with its thickness. Another factor in the effectiveness of a diffusion barrier is its crystallographic properties such as grain size and preferred crystalline orientation.

In electronic applications it is usual to deposit copper and/or copper alloy and tin in sequence. With a nickel diffusion barrier layer 0.5 um thick between the layers present, no failure occurs. Without the nickel layers between bronze, copper, or tin layers, for instance, intermetallic brittle layer(s) and Kirkendall voids are formed, leading eventually to separation of the coated system and substrate.

Also, when tin-containing solder connections are made to copper, intermetallic materials are formed. These materials keep growing to render weak surfaces. Again, a nickel layer between substrate and solder provides a solution to the problem.

1.12.5 Diffusion Welding

Here one utilizes diffusion to bring about joints of high quality. In other words, here, again, we have practical and useful aspects of thin-film interdiffusion. In practice, clean (very clean) cleaved or otherwise smoothened metal surfaces must be made for these to be in a firm mechanical contact while using a strong force that is still insufficient to cause macroscopic deformation even at an elevated temperature. This contact is usually done in vacuum or at least in an inert atmosphere. The problems of hard-to-reach joints and objectionable thermal conditions and the resultant undesired microstructures such as Kirkendall voids are minimized if not eliminated all together. Thus there can be achieved good-quality, distortion-free joints that require no additional machining or other posttreatment.

Often before welding can be performed, a special layer must be applied in the form of a thin-film coating or a thin foil in order to promote joining. Such coating can be applied by electroless or electrodeposition methods.

Five essential process variables common to all diffusion bonding techniques are to be considered: (1) temperature, (2) pressure, (3) time, (4) surface condition, and (5) process atmosphere.

Process temperature is usually one-half to three-fourths of the melting point of the lower melting point metal in the intended weld or bond. The purpose of attaining an elevated temperature is to promote or accelerate the interdiffusion of atoms at the joint interface and also to provide some metal softening, which in turn aids in surface deformation. The pressure application establishes a firm and robust mechanical contact of the surfaces and further breaks up surface oxides (hence the frequent use of silver). As a result, the surface is clean for bonding. The period of time at which the elevated temperature is maintained depends on metallurgical and other considerations.

1.12.6 Electromigration

In an electrical cord or wire, electricity is conducted without transport of atoms in the conductor. The common, free-electron model of electric conductivity makes a basic assumption that electrons are free to move in and through a metal lattice constrained only by scattering events. Scattering is the cause of electrical resistance and what is termed Joule heating. Scattening, however, does not cause displacement of atoms or ions as long as the current density is moderate. At high current densities (of about $10^4\,\mathrm{A\,cm^{-2}}$) the current can displace ions and thus cause transport of mass. The mass transport caused by the electric field and the charge carriers is known as *electromigration.* It is present in interconnecting lines in microelectronic devices, since in these lines the current density values are high. By way of example, a current of 2 mA applied to a 1-μm-wide aluminum line of 0.2 μm thickness, represents a current density value of $10^5\,\mathrm{A\,cm^{-2}}$; this current density will cause mass transport in the line even at room temperature. It constitutes a reliability failure endemic to thin-film circuits. As modern electronic circuitry becomes smaller and smaller, the current densities will become larger and the probability of circuit failure due to electromigration will be more of a problem. Both voids and extrusions can result. A line of aluminum that is subject to

an electric field and current density of sufficient magnitude can cause electromigration. The line can be expected to undergo morphological change such that depletion occurs at the negative (cathode) end while extrusion is present at the positive (anode) side. This means that the material migration is in the direction of the movement of the charge-carrying electrons. The driving force behind electromigration consists of two parts. The first is the direct action of the electrostatic field on the diffusing atoms. The second is the momentum exchange of the moving charge carriers with the diffusing atoms. These forces are referred to as the *direct* force and the *electron wind* force, respectively. The electron wind force is usually far greater than the direct force. There have been attempts to quantitatively, using quantum-mechanical methods, explain and estimate the electron wind force. None is widely accepted, and the common practice is to adhere to semiclassical treatments. Remedies include lowering the operating temperature or using other metals (than Al) that have a higher activation energy for diffusion where electromigration is less of a problem.

PART C MATERIALS SCIENCE OF ELECTRODEPOSITS

Electrodeposition has become a science capable of producing materials atom by atom with sophisticated, controllable structures and properties [32]. Historically, the structures formed have been characterized by the forms they take, such as grains, layers, needles, or a combination. Key aspects of electrodeposited materials that are relevant to the functional properties are grain dimension, preferred orientation, atomic density gradients, and composition. A high fraction of atoms in a granular electrodeposit are in interfacial zones. When grain size is in the 10–20-nm range, half the atoms are associated with grain boundaries or interfacial zones. These are high-energy regions, and since there is normally a large fraction of this material, the driving force for grain growth can be high.

Recently, electrodeposition has become a major nanotechnology enabler and benefits from application of modern analysis and processing methods [33, 34]. As an example, nanosized grains are produced in copper that is pulse plated or electrodeposited with direct current from baths containing complexing agents [35]. High-technology applications now include ultra-large-scale integration (ULSI) and microelectromechanical system (MEMS) packaging [36], thermoelectrics [37, 38], magnetics [39], and solar energy conversion [40, 41]. The improving nanotechnology theories and processes are combining with electrodeposition capabilities to give innovations such as stress-controlled structures [42], catalysts, and phase change materials [43].

1.13 STRUCTURE AND COMPOSITION

Electrodeposition yields a range of nano- and microstructures, depending on the material and the condition of deposition. In the majority of electrodeposited materials, the atoms are arranged in a uniform, three-dimensional array. The volume over which this arrangement extends uniformly is called a crystal. Most electrodeposits exist in one of three crystal habits: fcc, bcc, or hcp (see Part B).

When many crystals combine to form a solid material, they are called grains. If the array of atoms is random, the material is amorphous. However, in materials considered to be amorphous, there are generally still very small groups of atoms that possess the same arrangement as crystals [44].

Grain shape and size are determined by the plating conditions and the composition of the solution. If the grains are not randomly oriented, the condition is called a texture. In the case of electrodeposits the texture is a fiber axis because just as in a wire drawn through a die the directions perpendicular to the preferred orientation are randomly oriented. When electrodeposits are annealed, they generally recrystallize; that is, new grains form. When deposits recrystallize, the texture often changes. Simple plating solutions, such as acidified copper sulfate, produce large, columnar grains that generally exhibit a fiber axis. Solutions based on complex compounds, such as copper cyanide, or solutions containing active addition agents tend to yield fine-grained deposits that usually do not exhibit a texture.

There are defects in the crystalline arrangement. At the boundaries of grains there has to be a departure from the regular crystalline arrangement to accommodate different orientations or different crystal structures. Other defects in electrodeposits are primarily dislocations, twins, and codeposited foreign atoms or molecular groups. A dislocation is a line defect that can be thought of as being the boundary between a portion of a crystal plane that has been displaced by an applied force (i.e., slipped) and the portion that has not. However, dislocations can originate due to factors other than slip.

The density of dislocations in electrodeposits often approaches that of heavily, plastically deformed metals. Twins are a special type of grain that possesses two boundaries; the crystal arrangement on one side is the mirror image of that on the other side. Codeposited foreign atoms or molecular groups originate from intentional additions to the plating solutions or impurities in it.

Some deposits such as bright nickel show the so-called banded structure [45]. It manifests itself by a series of closely spaced, parallel lines seen in the cross section. It is caused by periodic variations of the overpotential. When the magnitude of the overpotential reaches its maximum value, growth is interrupted. This growth interruption appears as a line in the cross section. The periodicity of the interruptions results in the banded structure.

The substrate can affect the structure of the electrodeposit. If the interatomic distance in a particular crystal plane of the substrate closely matches that of a crystal plane of the deposit, the structure of the former may be continued into the latter (*epitaxy*). Oxides and other films on the substrate surface and distortions due to plastic flow from mechanical polishing hinder the development of epitaxy. Plating conditions that result in high overvoltages such as high current densities or certain additions to the plating solution are favorable to the formation of three-dimensional nuclei, that is, new grains. Then the relationship between the substrate and the deposit tends to be lost. On the other hand, elevated plating temperatures and low current densities favor epitaxial growth by allowing migration of atoms to sites where they can be incorporated into the existing structure.

There is a second way that substrate morphology can affect electrodeposit structure. Despite being cathodic, the substrate surface may dissolve in the plating solution and then redeposit with the plated metal as an alloy. Such is the case in some trivalent chromium plating solutions [46]. Etched substrate surfaces have been observed [47] to cause twins to form in the deposit.

Determining the structure and properties of electrodeposited materials entered a new phase with the emergence of nanotechnology as a field. Many electrodeposits are nanocrystalline or amorphous at the time of formation. Certain electrodeposit properties such as hardness, wear resistance, and electrical resistivity are strongly affected by grain size. Properties such as thermal expansion, Young's modulus, and saturation magnetization show little grain size dependence. Potential applications range from corrosion- and wear-resistant coatings to soft magnetic materials for magnetic recording.

1.13.1 Characterization

Microscopy and diffractometry are the main tools for determining the structure of electrodeposits. The transmission electron microscope permits measurement of structures on the nanoscale and is used to determine grain size. The scanning electron microscope is most widely used for monitoring deposit structures and chemical composition using X-ray fluorescence. X-ray diffraction (XRD) provides detailed structure information with less sample processing than is required for transmission electron microscopy (TEM). Scanning probe microscopes give the additional option for following electrodeposit growth in situ.

The transmission electron microscope has better resolution than the scanning electron microscope, with the capability to obtain electron diffraction patterns. By special techniques it is possible to obtain atomic resolution in TEM. The main disadvantage of TEM is that only very thin specimens can be examined. Thus extensive specimen preparation is required for most deposits.

With the transmission electron microscope, it is possible to determine the grain size unambiguously by placing the field-limiting aperature around an area believed to be a grain. Care must be taken that surrounding areas are not included by the aperature. An electron diffraction pattern is then obtained from the defined area. If the pattern is that of a single crystal, the area is a grain. The orientation of the grain as well as the direction in it can be determined from the diffraction pattern.

The scanning electron microscope is most frequently used for revealing the structure of electrodeposits. Its advantage over the optical microscope is a greater depth of field allowing a rough topography to be completely in focus. Surfaces that are electrically conducting can be examined with essentially no preparation. The scanning electron microscope also has better resolution than the optical one. The main disadvantage of SEM is that is is not possible to produce electron diffraction patterns. Thus the crystal structure and orientation of grains cannot be determined. Great care has to be taken when SEM is used to determine the grain size.

Most scanning electron microscopes have an attachment for chemical analysis by X-ray fluorescence. Because the electron beam can be focused on a small area, individual structural components can be chemically analyzed. Characteristic X rays can also be imaged so that the distribution of a particular chemical element can be seen.

When secondary electrons are used for imaging, nodules consisting of many crystallites can have the appearance of grains and be easily mistaken for them. It is possible to use backscattered electrons to image differences in orientation in the specimen and thus between grains. However, if there is a texture, which is frequently the case in electrodeposits, such a determination of grain size is difficult. The scanning electron microscope can also be operated to detect shorts in electrical circuits.

Recently a new class of scanning tunneling microscopes with resolution comparable to TEM has come into use for the study of the structure of electrodeposits. Their main advantage for the study of electrodeposits is that they can operate in liquids and can be used for in situ studies [48]. However, scanning tunneling microscopy (STM) cannot be used to observe continually changing processes because it takes a relatively long time to form an image. The tip is embedded in a cantilever beam. A laser measures the deflection of the beam and thereby the movement of the tip. The tunneling current controls the distance between the tip and the specimen surface in STM. A precisely controlled feedback system keeps the distance between the tip and the specimen surface constant, allowing it to follow the surface topography. Scanning tunneling microscopy has two disadvantages for studying electrodeposits. The tunneling current can affect the structure of an electrodeposit and all studied materials have to be electrical conductors.

The fiber axis is generally determined by XRD. The crystal direction perpendicular to the planes that result in

the highest intensity diffraction lines is usually taken as the fiber axis. Care must be taken to ensure that the preferred orientation is not a direction perpendicular to crystal planes that do not diffract, as, for example, the {211} planes of fcc metals.

Other methods used to characterize electrodeposits include:

- Differential Scanning Calorimetry (DSC) Phase transitions are detected using controlled measurement of temperature as heat is added or removed from a material.
- Scanning Electrochemical Microscopy (SECM) Chemical reactivity of a surface is mapped and monitored with a scanned probe. This is useful to evaluate materials for applications such as corrosion resistance.

1.14 PROPERTIES

1.14.1 Mechanical

The relevant mechanical properties are the modulus of elasticity; the yield, tensile, and fatigue strengths; and the ductility. The slope in the elastic portion is the modulus of elasticity. Yield strength is the stress to produce a small amount of plastic deformation called the *offset*. Tensile strength is the maximum stress. Ductility is the strain to fracture. Fatigue strength cannot be determined from a stress–strain curve. The mechanical properties are of particular importance for electroforms and printed circuits.

The two methods for determining the mechanical properties are the tensile and bulge tests. Tensile testing consists of applying a load continuously to a so-called dog-bone-shaped specimen until it fractures. The normally used tensile specimens are unsuitable for most electrodeposits. The 2-in.-wide reduced section of the standard tensile specimen has a width-to-thickness ratio that results in a nonuniform strain and therefore low values of the ductility [49].

Using a width-to-thickness ratio typical of the wiring of printed circuits and then scaling the other dimensions result in a tiny tensile specimen. Several machines to test such small specimens are in use [50]. The bulge test consists of clamping a foil over an orifice and introducing a fluid to cause a hemispherical bulge. A stress–strain curve can be constructed using measurements of the fluid pressure and the bulge height. The wiring of printed circuits, which are thermally cycled, can fail due to stresses that develop because of differences in the coefficients of thermal expansion between deposit and substrate. Thermal-cycling tests are used to test for such failures.

Sandia has developed a suite of mechanical properties measurements to measure stress–strain and fatigue properties of thin films used in MEMS fabrication. One documented example is Ni electrodeposited on metallized Si [51].

The moduli of elasticity of electrodeposits are generally smaller than those of the same metal formed in other ways. Possible reasons are the difficulty of obtaining accurate values and the possibility that deposits do not behave elastically.

The primary sources of strength are impediments to the movement of dislocations. In electrodeposits the main impediments are grain boundaries. Addition agents strengthen deposits primarily by refining the grains. Codeposited foreign substances can also increase the dislocation density. Dislocations can hinder the movement of others and thus strengthen materials.

Ductility is the amount of plastic deformation that can occur prior to fracture. Some deposits are inherently brittle because they contain cracks that readily lead to fracture. The cracks can be caused by the internal stresses, which will be subsequently discussed, and by stress corrosion.

Fine-grained deposits tend to be brittle because plastic deformation that occurs primarily by dislocation motion is impeded by the grain boundaries. Some deposits appear to be brittle but are really quite ductile. The reason for this behavior is a phenomenom called *necking*. Here the plastic deformation prior to fracture occurs in a very small volume. The overall plastic deformation is then quite small and thus indicative of poor ductility. However, the ductility, as indicated by the reduction in the cross-sectional area prior to fracture, may be quite good. When the deposit adheres well to the substrate, necking is essentially prevented.

Annealing of electrodeposits is mostly a low-temperature heat treatment to remove hydrogen, which can be a source of embrittlement. Electroforms may be heat treated so as to cause recrystallization. The recrystallization temperature of electrodeposits is generally lower than that of the same wrought metals. Some fine-grained copper electrodeposits have been observed by the author to recrystallize at ambient temperatures.

Precipitation hardening is possible for some supersaturated solid solution. Electroless nickel is an example of such an alloy that can be heat treated to cause the precipitation of Ni_3P or Ni_3B and thereby substantially increase the hardness and wear resistance [52].

Electrodeposition is well suited for the production of composites. The incorporation of hard material such as diamonds or ceramic particles can markedly improve the wear resistance. Composites consisting of thin alternate layers of two different materials can possess better strength properties than those of the individual ones. Composites have been produced consisting of alternate layers of two different metals such as nickel and copper, layers of alloys of different composition, or layers of different phases such as alpha and beta brass. These composites have been produced in one solution by alternately changing the plating conditions rather than by plating in two different solutions, which is impractical.

1.14.2 Magnetic

Allongue et al. [39] have demonstrated that electrodeposition can provide high-quality, epitaxial, ultrathin, magnetic layers with perpendicular magnetic anisotropy. This allows control of magnetism on a nanometer scale. The Allongue group also found that Co electrodeposited on Au(111) shows enhanced perpendicular magnetization anisotropy which is of interest for magnetic data storage [53].

Magnetic materials are classified as hard or soft depending on the value of the coercive force. Materials with coercive forces exceeding 200 Oe are considered magnetically hard. They are used, for example, in disc elements for information storage. Electroless cobalt–phosphorus alloys are magnetically hard materials. When it is desired that relatively low fields are capable of switching from cine remanence state to another, for example, as in plated-wire memory elements, magnetically soft materials are used. Examples of magnetically soft materials are iron–nickel alloys. A high remanence and a square hysteresis loop are desirable for both types of materials.

The principal structural element in magnetism is the domain. It is a small region that has a spontaneous magnetization. The sizes of domains vary greatly. For information storage, the domains should be as small as possible; their size is then limited by the width of their walls, which is less than 1 μm. At the other extreme, a whole magnet can be one domain. If the magnetization directions of all domains are randomly oriented, there is no net bulk magnetization. The effect of an imposed field is to align domains along its direction.

Domains already aligned grow at the expense of less favorably oriented ones by moving their walls. At the saturation magnetization, the only existing domains are those oriented in the proper direction. Since domains do not completely revert to the random orientation when the field is removed, there is remenance. The coercive force is that required to cause a random orientation of the magnetization directions of the various domains. A ferromagnetic element used for storing information is in either the positive or the negative remenence state, which constitutes its memory. The magnitude of the magnetization decreases drastically when the material is heated to the Curie temperature.

The microstructure of electrodeposited materials affects the magnetic properties in several ways. The previously discussed defects, namely dislocations, grain and twin boundaries, and some codeposited materials, make it more difficult for domain walls to move, and this results in higher coercive forces. The ease of moving domains also depends on the crystallographic orientations. Since each magnetic material possesses a particular orientation in which it is most easily magnetized, the texture is in this case of practical importance.

When a material is magnetized, its shape and volume change. The change, which is called *magnetostriction*, is due to a strain resulting from the magnetization. Magnetostriction can also be a change in the magnetization due to strains. When deposition occurs in a magnetic field, the structure, texture, and throwing power of both magnetic and nonmagnetic materials can be affected.

1.14.3 Internal Stress

Electrodeposits are often laid down in a state of stress termed either internal or residual because all or part of it remains in the deposit. Electroplaters are familiar with macrostress, as it manifests itself in the bending of parts plated on one side. If one end of a strip is clamped and the other one bends toward where the anode was located, the macrostress is tensile. If the strip bends in the opposite way, the macrostress is compressive. Macrostresses can cause distortions, cracking of the deposit, loss of adhesion to the substrate, and increased corrosion. Tensile macrostresses can also deteriorate the fatigue properties. The other type of stress—microstress—manifests itself primarily in an increase in the hardness.

The most commonly commercially used macrostress-measuring device is the spiral contractometer. The problem with devices such as the contractometer in which the specimen is allowed to deform is that some of the stress is relieved. There are devices used in research in which an opposing force is applied so as not to allow the specimen to deform. Microstresses can be determined only from the broadening of XRD lines. X-ray diffraction can also be used to measure macrostresses. However, it usually does not yield accurate values for electrodeposits because of the broadening of the diffraction lines due to microstresses and their symmetry due to twinning.

The structural causes of internal macrostresses are not fully understood. There is evidence that the coalescence of grains or parts of them growing laterally from different nucleation centers is a cause. The stress fields around oriented arrays of dislocation produced by coalescence or other growth processes can add in such a way as to result in macrostresses. The sign of the macrostress depends on the orientation of the array. The codeposition of hydrogen has been identified as a cause of macrostress.

If hydrogen diffuses out of a layer of the deposit allowing it to shrink, a tensile macrostress can develop. A tensile macrostress can also develop if hydrogen diffuses onto the substrate or previously laid-down layers causing them to expand. If micropores form during deposition and hydrogen then diffuses into them, causing them to expand, a compressive macrostress can be caused.

Polycrystalline thin films develop intrinsic stress, which can impede applications. As an example, the Sandia group determined that stress level tends to stabilize within the first 200 nm of film growth [54].

1.14.4 Hardness

The most frequently conducted test of the properties of electrodeposits that may be indicative of the strength and ductility is that of hardness. Hardness readings are of value when they have been experimentally related to the strength or ductility of a specific material. They can also be useful as an indication of wear resistance.

For electrodeposits, even the qualitative relationships commonly observed among hardness, tensile strength, and ductility do not always prevail. For example, it would be expected that hardness increases with tensile strength and decreases with ductility. However, the reverse effect is common among electrodeposits. It is particularly important, therefore, in dealing with deposits to be sure of the significance of the hardness values.

The most commonly performed hardness test is the indention test. It consists of pushing an indentor into the material via an applied load. The diameter or diagonal of the indent is measured with a microscope having a filar eyepiece. The indention is generally made on the cross section because the thickness of the coating has to be at east 14 times greater than the depth of the indent. Failing this requirement, the substrate affects the hardness value by what is commonly called the anvil effect.

The largest indent on the cross section for the greatest accuracy is obtained with the Knoop indentor, which is a symmetric, pyramidal, diamond point. It produces an indent whose length is about 7 times its width and 30 times its depth. The length of the indent should be, of course, parallel to the substrate–deposit interface. The Vickers indentor, which produces an indent whose length and width are equal, is also used for deposits. The nanohardness tester produces such a small indent that it can be used on the surface without causing the anvil effect. Since the hardness depends on the applied load, it should always be specified.

The useful Hall–Petch correlation tends to break for extremely small grain size. In one study of electrodeposited Ni and Co, the materials appear to strain harden and have reduced tensile strength when nanocrystal size decreases to the 5–20-nm range [55].

1.14.5 Adhesion

Adhesion can be regarded as the degree to which a bond has been developed from place to place at the coating–substrate interface. The strength of such a bond should equal or exceed the cohesive strength of the weaker of the two materials involved. Adhesion of metallic substrates is generally better than is required for normal service. Plating on plastics can present a serious adhesion problem.

There are several accepted methods for evaluating adhesion of electrodeposited coatings [32], Generally, the coating is pulled off mechanically, and tests should be performed with production items rather than test specimens where possible.

The Ollard test for bonding consists of plating a metal cylinder to a thickness of about 2.5 mm and then machining the deposit so as to leave a shoulder that is supported by a die. A load is applied to separate the deposit from the substrate and is indicative of the bond strength. Roehl [56] refined Ollard's method and extensively studied nickel on steel. His work and other investigations indicated that the bond strength equals or exceeds the cohesive strength of the weaker of the two involved metals.

Fracture rarely occurs at the interface if a good plating technique was employed. If the load is applied perpendicular to the deposit–substrate interface, the value of the bond strength is more quantitative. To apply the load in this way, a nodule shaped by an electroforming technique is deposited on the substrate and subsequently pulled off. The bond strength is then the load needed to pull off the nodule divided by its area.

The main factor that is detrimental to adhesion is a brittle layer which can form by diffusion between the deposit and substrate. Brittle layers form especially if annealing is involved. An example is copper plated on zinc die castings, which forms blisters during the baking of enamels applied over the coating.

1.15 APPLICATIONS

Electrodeposited thin films are playing a major role in the development of new magnetic materials. Allongue and his group [39] are developing a picture of epitaxial growth and magnetism for ultrathin magnetic layers, such as Ni, Co, and Fe on Au(111). Their research supports development of both bit-patterned storage media where each nanostructure will bear one bit of information and magnetic random-access memory.

Thermoelectric devices are another emerging technology that uses electrodeposited materials [38]. Nanostructured deposits of the alloys of bismuth, antimony, tellurium, and select other elements have useful thermoelectric properties. One successful fabrication technique is to electrodeposit the materials into nanoscale pores [37]. Thermoelectrics are an important energy conservation enabler for turning waste heat into useful electricity.

Electrodeposition of materials that can change phase on heating or cooling is opening up new application opportunities. In one example, SbTe is deposited in the amorphous state at room temperature. On heating, the film crystallizes to Sb_2Te_3 at 120°C. This switching between amorphous and crystalline forms is potentially useful for rewritable optical storage and solid-state memory [43].

Electrolytic deposition is uniquely suited to produce the wiring of printed circuits and the interconnections of multilayer microchips. By the use of photoresist, the areas to be plated can be precisely defined. Autocatalytics, known as electroless plating, permit a conducting layer to be deposited on insulating materials. Thin layers of solder can be deposited for making connections. Some unique materials for use in electronic applications have been developed. Of special importance are materials having structures on the nanometer scale [36].

REFERENCES

1. M. Paunovic and M. Schlesinger, *Fundamentals of Electrochemical Deposition*, Wiley, New York, 1998 and 2006.
2. J. O'M. Bockris and A. K. N. Reddy, *Modern Electrochemistry*, Vol. 1, Plenum, New York, 1998.
3. E. Mattsson and J. O'M. Bockris, *Trans. Faraday Soc*, **55**, 1586 (1959).
4. A. J. Bard and L. R. Faulkner, *Electrochemical Methods*, Wiley, New York, 1980.
5. W. Lorenz, *Z. Phys. Chem.*, **202B**, 275 (1953).
6. W. Lorenz, *Z. Elektrochem.*, **57**, 382 (1953).
7. W. Lorenz, *Naturwissenschaften*, **40**, 576 (1953).
8. W. J. Lorenz, *Z. Naturforsch*, **9a**, 716 (1954).
9. W. Mehl and J. O'M. Bockris, *J. Chem. Phys.*, **27**, 817 (1957).
10. W. Mehl and J. O'M. Bockris, *Can. J. Chem.*, **37**, 190 (1959).
11. B. E. Conway and J. O'M. Bockris, *Proc. Roy. Soc. London*, **A248**, 394 (1958).
12. B. E. Conway and J. O'M. Bockris, *Electrochim. Acta*, **3**, 340 (1961).
13. G. H. Gilmer and P. Bennema, *J. Appl. Phys.*, **43**, 1347 (1972).
14. N. Ibl, *Surf. Technol.*, **10**, 81 (1980).
15. A. M. Pesco and H. Y. Cheh, in *Modern Aspects of Electrochemistry*, No. 19, B. E. Conway, J. O'M. Bockris, and R. E. White, Eds., Plenum, New York, 1989.
16. C. H. Ting, V. Dubin, and R. Cheung, in *Fundamental Aspects of Electrochemical Deposition and Dissolution Including Modeling*, M. Paunovic, M. Datta, M. Matlosz, T. Osaka, and J. B. Talbot, Eds., *Proceedings,* Vol. 97-27, Electrochemical Society, Pennington, NJ, 1997, p. 321.
17. E. Budevski, G. Staikov, and W. J. Lorenz, *Electrochemical Phase Formation and Growth*, VCH Publishers, New York, 1996.
18. D. J. Srolovitz, A. Mazor, and G. G. Bukiet, *J. Vac. Sci. Technol.*, **A6**, 2371 (1988).
19. A. Damjanovic, M. Paunovic, and J. O'M. Bockris, *J. Electroanal. Chem.*, **9**, 93 (1965).
20. J. O. Dukovic and C. Tobias, *J. Electrochem. Soc.*, **137**, 3748 (1990).
21. C. Madore and D. Landolt, *J. Electrochem. Soc.*, **143**, 3936 (1996).
22. H. Leidheiser Jr., *Z. Elektrochemie*, **59**, 756 (1955).
23. O. Kardos and D. G. Foulke, in *Advances in Electrochemistry and Electrochemical Engineering*, Vol. 2, C. W. Tobia, Ed., Wiley-Interscience, New York, 1962.
24. R. Weil and R. Paquin, *J. Electrochem. Soc.*, **107**, 87 (1960).
25. L. Oniciu and J. Muresan, *J. Appl. Electrochem.*, **21**, 565 (1991).
26. G. T. Rogers and K. J. Taylor, *Electrochim. Acta*, **8**, 887 (1963); **11**, 1685 (1966); **13**, 109 (1968).
27. M. Paunovic, *Plating*, **55**, 1161 (1968).
28. M. Satto, *J. Met. Fin. Soc. Jpn.*, **17**, 14 (1966).
29. M. Paunovic, in *Electrochemistry in Transition*, O. J. Murphy, S. Srinivasan, and B. E. Conway, Eds., Plenum, New York, 1992, p. 479. [29a] M. Yoshino, T. Masuda, T. Yokoshima, J. Sasono, Y. Shacham-Diamand, I. Matsuda, T. Osaka, Y. Hagiwara, and I. Sato, *J. Electrochem. Soc.*, **154** (3), D122 (2007). [29b] J. W. Gallaway and A. C. West, *J. Electrochem. Soc.*, **155**, D632 (2008). [29c] R. Manu and S. Jayakrishnan, *J. Electrochem. Soc.*, **156** (7), D215 (2009).
30. A. Brenner, Ph.D. Thesis, University of Maryland, 1939.
31. J. Yahalom and O. Zadok, *J. Mater. Sci.*, **22**, 499 (1987).
32. W. Dini, *Electrodeposition: The Materials Science of Coatings and Substrates*, Noyes, New York, 1993.
33. I. Gurrappa and L. Ginder, *Sci. Technol. Adv. Mater.*, **9**, 043001 (2008).
34. S. C. Tjong and H. Chen, *Mater. Sci. Eng.*, **R45**, 1 (2004).
35. L. P. Bicelli et al., *Int. J. Electrochem. Sci.*, **3**, 356 (2008).
36. M. Datta and D. Landolt, *Electrochim. Acta*, **45**, 2535 (2000).
37. E. Kouiharenko et al., *J. Micromech. Microeng.*, **18**, 104015 (2008).
38. F. Xiao et al., *Electrochim. Acta*, **53**, 8103 (2008).
39. P. Allongue et al., *Surf. Sci.*, **603**, 1831 (2009).
40. K. Kajeshwar, N. R. de Tacconi and C. R. Chenthamarakshan, *Curr. Opin. Solid State Mater. Sci.*, **8**, 173 (2005).
41. I. M. Dharmadasa and J. Haigh, *J. Electrochem. Soc.*, **153** (1), G47 (2006).
42. C. C. Koch, *J. Phys. Conf. Ser.*, **l44**, 012081 (2009).
43. Q. Huang, A. J. Kellock, and S. Ranoux, *J. Electrochem. Soc.*, **155** (2), D104 (2008).
44. R. Weil and K. Parker, in *Elctroless Plating*, G. O. Mallory and J. B. Hajdu, Eds., American Electroplaters and Surface Finishers Society, Orlando, FL, 1990, pp. 111–138.
45. C. C. Nee and R. Weil, *Surf. Technol.*, **25**, 7 (1985).
46. C. Sheu and R. Weil, *J. Electrochem. Soc.*, **137**, 2052 (1990).
47. E. C. Felder, S. Nakahara, and R. Weil, *Thin Solid Films*, **84**, 197 (1981).
48. C. J. Weber, H. W. Pickering, and K. G. Weil, *J. Electrochem. Soc.*, **144**, 2364 (1997).
49. K. Lin, I. Kim, and R. J. Weil, *Plating Surf. Finish.*, **75**, 52 (1988).

50. Kim and R. Weil, in *Testing of Metallic and Inorganic Coatings*, ASTM **STP** 947, W. B. Harding and G. DiBari, Eds., American Society for Testing and Materials, Philadelphia, PA, 1987, pp. 11–18.
51. S. J. Hearne et al., Report SAND 2005-7067, Sandia National Laboratories, Albuquerque, NM, 2005.
52. R. J. Weil and K. Parker, in *Electroless Plating*, G. O. Mallory and J. B. Hajdu, Eds., American Electroplaters and Surface Finishers Society, Orlando, FL, 1990, p. 111.
53. P. Prudhomme et al., Abstract 293, Presented at the 207th ECS Meeting, 2005.
54. A. Bhandari, B. W. Sheldon, and S. J. Hearne, *J. Appl. Phys.*, **101** (3), 033528 (2007).
55. L. Brooks et al., *Mater. Sci. Eng.*, **A491**, 412 (2008).
56. E. J. Roehl, *Iron Age*, **146** (13), 17 (1940); **146** (14), 30 (1940).